Geological Magazine

www.cambridge.org/geo

The Sr, Nd, Pb and Hf isotopes and crystallization conditions of the middle Eocene Dağdibi Pluton in the eastern Sakarya Zone, Turkey

Ferkan Sipahi[1], Mehmet Ali Gücer[1], Abdurrahman Dokuz[1], Keewook Yi[2], Abdullah Kaygusuz[1], Enver Akaryalı[1], Çiğdem Saydam Eker[1] and Cüneyt Doruk[3]

[1]Department of Geological Engineering, Gümüşhane University, Gümüşhane, Turkey; [2]Geochronology Team, Korea Basic Science Institute, Chungbuk, South Korea and [3]Gümüşhane University, Graduate Education Institute, Gümüşhane, Turkey

Original Article

Cite this article: Sipahi F, Gücer MA, Dokuz A, Yi K, Kaygusuz A, Akaryalı E, Saydam Eker Ç, and Doruk C (2023) The Sr, Nd, Pb and Hf isotopes and crystallization conditions of the middle Eocene Dağdibi Pluton in the eastern Sakarya Zone, Turkey. *Geological Magazine* **160**: 1193–1210. https://doi.org/10.1017/S001675682300033X

Received: 9 August 2022
Revised: 25 April 2023
Accepted: 16 May 2023
First published online: 7 June 2023

Keywords:
Eocene; Hf Isotope; non-adakitic Pluton; Sr–Nd–Pb isotopes; Sakarya Zone; Turkey

Corresponding author: F. Sipahi;
Email: ferkansipahi@gmail.com

Abstract

Magmatic activity in the Sakarya Zone, an important segment of the Alpine orogenic belt, continues intermittently from the middle Carboniferous to Miocene. In this study, we provide geochronological and geochemical data from the Dağdibi Pluton in the eastern Sakarya Zone to present some inferences on the source region and petrogenesis of the middle Eocene magmatism. U–Pb zircon geochronology from two granodiorite samples gives middle Eocene ages of 44.75 ± 0.92 and 45.01 ± 0.59 Ma. The pluton is mainly composed of K-feldspar, plagioclase, quartz, Mg-hornblende/actinolite, Fe–Ti oxides and small amounts of biotite, and secondary chlorite and epidote. Parental magma of the intrusive rocks has a high-K calc-alkaline affinity with metaluminous character. The oxygen fugacity values vary between −18 and −17. The rocks show slightly radiogenic $^{87}Sr/^{86}Sr_{(i)}$ (0.704845–0.705726) ratios and ϵNd_i values between −0.96 and +0.52. Pb–Pb isotope ratios are typical for those of the lower continental crust. $\epsilon Hf_{(i)}$ values of the zircons range from 0.14 to 10.26. The geochemical and isotopic features of the pluton point to a parental magma derived from a depleted mantle that was metasomatized by fluids during previous subduction events. The volumetric abundances of the rock types are decreased as the silica content increase, implying that the fractional crystallization is the most important process during the formation of the present compositional range of the pluton. Amphibole, plagioclase and Fe–Ti oxides are the fractionated phases while K-feldspar is largely accumulated. In the light of the data presented above, slab breakoff is regarded as the geodynamic process responsible for the formation of the Dağdibi Pluton in the middle Eocene.

1. Introduction

The Dağdibi Pluton is located in the eastern part of the Sakarya Zone, Turkey, a crustal segment lying in the middle parts of the Alpine-Himalayan Orogenic Belt. Although the igneous rocks with ages varying from Carboniferous to Miocene are found in the eastern Sakarya Zone, those formed in the time interval from the Late Cretaceous to the end of Eocene are very common (Sipahi, 2005, 2017, 2019; Arslan & Aslan, 2006; Boztuğ *et al.* 2007; Kaygusuz *et al.* 2012, 2018, 2020; Temizel *et al.* 2012; Aydınçakır, 2014; Sipahi & Sadıklar, 2014; Gücer *et al.* 2017; Dokuz *et al.* 2019; Sipahi *et al.* 2020a, 2020b, 2022; Gücer, 2021). Particularly the eastern part of the Sakarya Zone is therefore regarded as a paleo-magmatic arc and a natural laboratory to study the tectonic and petrogenetic processes that occurred through the time interval from the final stages of subduction to post-collision. Geochemical data are widely used to discriminate the tectonic settings of igneous rocks during their formation. However, magmas formed during active subduction and collision can bear similar geochemical compositions because their trace element budgets are closely related to their abundance in protolith (e.g., Roberts & Clemens 1993; Dokuz *et al.* 2019). Thus, additional data from other disciplines, such as structural geology, stratigraphy and sedimentology, are needed to arrive at a realistic tectonic setting for magmatic rocks.

Although there are plenty of studies on the Eocene igneous rocks in the eastern Sakarya Zone (Fig. 1a), the cause of the Eocene magmatism is still not fully understood. Late Cretaceous subduction-related magmatism was followed, after a magmatic stagnation of ~10–12 Ma, by a short-lived adakitic magmatism that occurred in a time span from 56 to 50 Ma with a peak at around 52–50 Ma (Karslı *et al.* 2010; Eyüboğlu *et al.* 2011; Dokuz *et al.* 2013; Gücer, 2021) and then a non-adakitic magmatism varying in age from 50 to 38 Ma (Boztuğ *et al.* 2004; Arslan & Aslan, 2006; Karslı *et al.* 2012; Eyüboğlu *et al.* 2017; Sipahi *et al.* 2017; Kaygusuz *et al.* 2018; Dokuz *et al.* 2019; Sipahi *et al.* 2022).

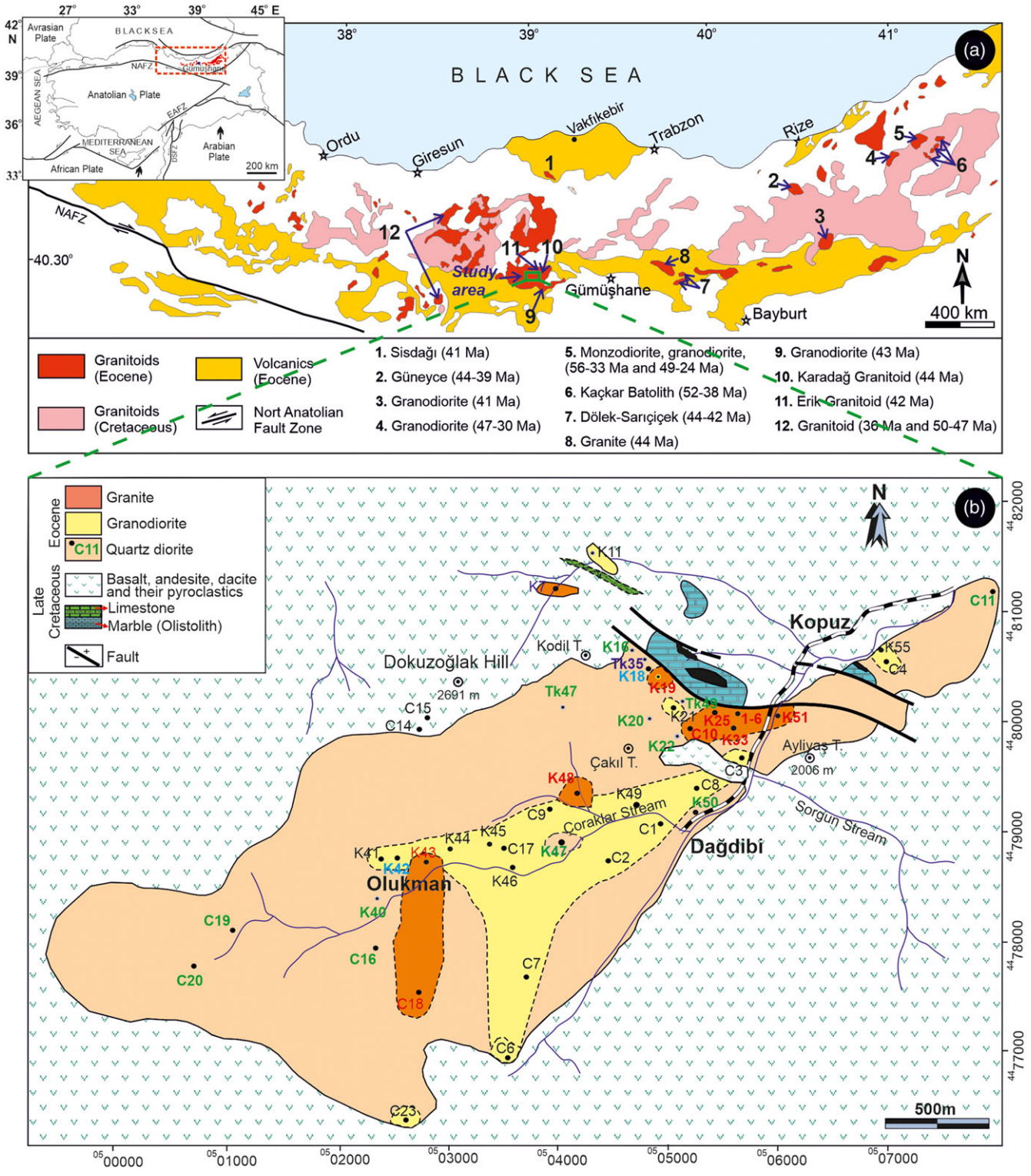

Figure 1. (Colour online) (a) Distributions of the plutonic rocks of Late Cretaceous and Eocene ages in the eastern part of the Sakarya Zone and (b) Geological map of the Dağdibi Pluton and surrounding area. **1**: Karslı *et al.* (2012); **2**: Taner (1977); **3**: Moore *et al.* (1980); **4**: Çınar (1975); **5**: Delaloye *et al.* (1972); **6**: Boztuğ *et al.* (2007); **7**: Karslı *et al.* (2007); **8**: Arslan & Aslan (2006); **9**: JICA (1986); **10**: Sipahi *et al.* (2022); **11**: Sipahi *et al.* (2017); **12**: Boztuğ *et al.* (2004).

The Dağdibi Pluton is one of the members of the middle Eocene non-adakitic plutons. We present U–Pb zircon geochronology, whole-rock geochemistry, Sr–Nd–Pb isotopes and microprobe data to contribute to our understanding of petrogenetic and geodynamic processes acted during the middle Eocene magmatism.

https://doi.org/10.1017/S001675682300033X Published online by Cambridge University Press

2. Geological setting

Basement rocks of the Sakarya Zone are represented by early Carboniferous metamorphic rocks (Topuz *et al.* 2007; Dokuz *et al.* 2022), and middle to late Carboniferous granitic (Dokuz, 2011; Kaygusuz *et al.* 2012) and rhyolitic rocks (Dokuz *et al.* 2017a). The basement metamorphic and rhyolitic rocks are unconformably overlain by the upper Carboniferous sedimentary rocks (Okay & Leven, 1996; Dokuz *et al.* 2023). Late Permian and Triassic rocks, which are common as allochthonous blocks within the accretionary complexes of the central and western Sakarya Zone, are absent in the eastern Sakarya Zone. The time period from the Late Triassic to Early Jurassic is regarded as the birth of the Neotethys Ocean behind the ribbon-shaped Cimmerian Continent, which was separated from the northern margin of Gondwana during the closure of the Paleotethys Ocean (Şengör & Yılmaz, 1981; Dokuz & Sünnetçi, 2019). The Early Jurassic is represented by sedimentary and basic volcanic rocks that lie unconformably over the Variscan basement (Dokuz & Tanyolu, 2006) and some basic to intermediate plutonic rocks (Dokuz *et al.* 2006; Eyüboğlu *et al.* 2016; Karslı *et al.* 2017). The Late Jurassic-Early Cretaceous period is characterized by platform-type carbonates and few magmatic rocks (Dokuz *et al.* 2017b).

The sedimentary rocks deposited in the Late Cretaceous in the eastern Sakarya Zone show distinct facies differences from north to south related to the northward subduction of the Neotethyan oceanic lithosphere (Yılmaz & Boztuğ, 1996; Şengör *et al.* 2003; Sipahi & Sadıklar, 2014; Kandemir *et al.* 2019). A sedimentary succession in the fore-arc side to the south temporally corresponds to at least four different volcano-sedimentary units in the back-arc side to the north (Aydin *et al.* 2020; Oğuz-Saka *et al.* 2023). Upper Cretaceous granitic rocks are dominated in the inner-arc environment of the eastern Sakarya Zone (Yılmaz & Boztuğ, 1996; Şengör *et al.* 2003; Sipahi *et al.* 2018a).

Adakitic rocks emplaced approximately 10–12 Ma after the collision of the Anatolides with Sakarya Zone are a single rock-record formed in the late Palaeocene to early Eocene period (Topuz *et al.* 2005; Eyüboğlu *et al.* 2011; Dokuz *et al.* 2013). Non-adakitic magmatic rocks began to form in the region almost coevally with the final stage of the adakitic rocks (Aydınçakır, 2014) and continued to middle Eocene (Arslan *et al.* 2013). The middle Eocene units in the eastern Sakarya Zone crop out in east-west trending semi-isolated areas and are represented mainly by volcano-sedimentary rocks. Basalt, andesite and lesser trachytes with a predominantly calc-alkaline to some alkaline geochemical tendencies are the dominant rock types (Arslan and Aslan, 2006; Temizel *et al.* 2012; Göçmengil *et al.* 2018). The Eocene plutonic rocks with a compositional range from gabbro to granite are more common in the central to northern parts of the eastern Sakarya Zone and offer similar geochemical characteristics with those of the extrusive rocks (Eyüboğlu *et al.* 2016, 2017; Dokuz *et al.* 2019; Sipahi *et al.* 2022).

The Dağdibi Pluton intruded into the Upper Cretaceous volcanic and sedimentary rocks. The volcanic rocks comprise basalt, andesite, dacite and associated pyroclastic rocks (Figs. 1b and 2). Sedimentary rocks consist of grey sandy limestone and limestone. The Upper Cretaceous limestone includes olistoliths of the Upper Jurassic-Early Cretaceous low-grade contact metamorphic limestone. The Dağdibi Pluton, which is the youngest unit of the study area, cuts all the older units (Figs. 1b and 2a) and crops out in an area of about 12 km^2 with an oval shape extending in southwest–northeast directions (Fig. 1b). The pluton contains mafic microgranular enclaves ranging in size from 0.5 to 5 cm. They are angular in shape and darker in colour and have finer-grained texture than their host pluton. A skarn zone was developed at the limestone contact of the pluton in the eastern boundary. Along this contact, the limestone was transformed into marble and in places recrystallized.

3. Analytical methods

U–Pb Ages: The U–Pb zircon geochronology of the selected samples was performed at the Korea Basic Science Institute Laboratory (South Korea). Cathodoluminescence (CL) images were taken to determine the points to be analyzed on the zircon grains and to control the internal structures of zircon grains. Zircon U–Th–Pb isotopes were measured using SHRIMP (Sensitive High-Resolution Ion Microprobe) IIe/MC at the Korea Basic Science Institute. A 2–4 nA mass-filtered O_2 primary beam was focussed on an elliptical spot with a diameter of 20 × 25 μm with a 120 μ Kohler aperture on the polished surface of the zircon with an accelerating voltage of 10 kV. Each spot was scanned with a primary beam for 2–3 min prior to analysis and then analyzed with a single electron multiplier for five cycles. FC1 (1099 Ma; Paces & Miller, 1993) and SL13 ($U = 238$ ppm) standard zircons were used for Pb/U calibration and U abundances, respectively. Th/U ratios were calculated using a fractionation factor derived from $^{232}Th^{16}O^+/^{238}U^{16}O^+$ measured against $^{208}Pb/^{206}Pb$ of the SL13 standard, while Pb/U ratios were calibrated against FC1 using the power law relationship between Pb^+/U^+ and UO^+/U^+. Common Pb was removed by the correction method of ^{207}Pb (<1000 Ma for dates) or ^{204}Pb (>1000 Ma for dates) using the model of Stacey & Kramers (1975). Data processing was carried out using SQUID 2.50 and Isoplot 4.15 programs running under Excel® (Ludwig, 2012). Zircons with high U concentrations (>2500 ppm) were corrected using the algorithm of Williams & Hergt (2000).

Whole Rock Geochemistry: Representative samples were selected for major, trace, and rare earth element (REE) analyses at the commercial ACME Laboratories, Ltd., Vancouver, Canada. Major elements were measured with inductively coupled plasma–atomic emission spectrometry after fusion with $LiBO_2$. The 0.2 g of powder sample and 1.5 g of $LiBO_2$ flux were mixed in a graphite crucible and subsequently heated to 1050°C for 15 min for trace elements and REE analyses. ICP-AES was used to measure major oxide elements and ICP-MS to measure trace and REEs.

Mineral Chemistry: Microprobe analyses were made on five samples from the studied pluton at the Geology and Mineral Research Laboratory of the New Mexico Institute of Mining and Technology, USA. Plagioclase, K-feldspar, biotite, amphibole, pyroxene and Fe-Ti oxide minerals were analyzed using a CAMECA-SX 100 brand microprobe-3 wavelength dispersive (WD) spectrometry device. The device worked with the 15 kV voltage and 20 nA.

Sr, Nd, Pb isotopes Analysis: Rb–Sr, Sm–Nd, and Pb–Pb isotope geochemistry analyzes of five samples were performed with Thermal Ionization Mass Spectrometry (TIMS) Laboratory at New Mexico State University (USA). Isotopic measurements were made by TIMS on a VG Sector 30 mass spectrometer. Samples analyzed were loaded on rhenium layers either on monofilament Cathodian beads only or on the sidewall of the triple filament junction. The repeatability of the $^{87}Rb/^{86}Sr$ and $^{147}Sm/^{144}Nd$ ratios is within 0.3% and the $^{87}Sr/^{86}Sr$ and $^{143}Nd/^{144}Nd$ ratios are within ±0.0000025

https://doi.org/10.1017/S001675682300033X Published online by Cambridge University Press

Figure 2. (Colour online) Field, outcrop and hand-sample photos of the studied pluton. (a) Contact between granodiorite, marble and volcanic rocks (C3, K-21), (b) Diorite (C8B) and (c) Hand-sample of granite.

and ±0.00003, respectively. An analysis of the NBS 987 standard yielded values of 0.710226 (11), 0.710213 (13), 0.710219 (10), and 0.710260 (11). Pb samples were analyzed using the middle filament position of a set of Cathode beads. The samples were loaded in a matrix of silica gel and phosphoric acid and using 5% HNO_3. Approximately 2 µL of silica gel was placed on the filament and 1 µL of phosphoric acid was added. Standards were also loaded and analyzed using the same procedures. The average of standard treatments was determined as $^{206}Pb/^{204}Pb = 16.844$, $^{207}Pb/^{204}Pb = 15.379$ and $^{208}Pb/^{204}Pb = 36.199$. The deviations from the standards are within 0.2%. Ramos (1992) provided detailed analytical procedures for isotopic measurements of Sr and Nd.

Lu–Hf isotope Analysis: Lu–Hf isotope analysis on single zircons of the pluton was made using a LA-MC-ICPMS with Nu Plasma II, Nu instruments + New Wave Research 193 nM ArF, ESI at the Korea Basic Science Institute (KBSI). Instrument parameters include a spot size 50 µm, a 10 Hz repetition rate, and energy density of 6–8 J/cm^2, dwell time 60 s for Hf isotope analysis of zircon. The interference of ^{176}Lu and ^{176}Yb on the ^{176}Hf signal was corrected by using Chu *et al.* (2002) and Vervoort *et al.* (2004), respectively. Mass bias of measured Hf isotopic ratios was corrected to $^{179}Hf/^{177}Hf = 0.7325$, using an exponential correction law (Russel *et al.* 1978; Patchett *et al.* 1981). The $^{176}Lu/^{177}Hf$ and $^{176}Yb/^{177}Hf$ ratios were calculated after Iizuka & Hirata (2005). Data reduction was carried out using Iolite 2.5 running within Igor Pro 6.3.5.5 software program (Paton *et al.* 2011). All ratios were calculated with 2σ errors. During the sample analysis, to evaluate the precision and accuracy of $^{176}Hf/^{177}Hf$ ratios, two reference zircons 91500 (0.282297; Griffin *et al.* 2000) and Plešovice (0.282482; Sláma *et al.* 2008) were repeatedly analyzed at the beginning and end of each analytical session, and at regular intervals during session.

4. Results

4.a. Petrography

The contacts of the Dağdibi Pluton are discordant with surrounding rocks (Fig. 2). Fe skarn mineralization was developed between the pluton and limestone–andesite contact in the Kopuz area (Sipahi *et al.* 2018b).

The Dağdibi Pluton consists, in decreasing order of abundance, of quartz diorite, granodiorite and granite with a zonal structure. The granodiorite and granite are located in the central portions of the pluton (see Fig. 1b). The rocks of the pluton show medium-grained, monzonitic, poikilitic and micrographic textures. Orthoclase, plagioclase ($An_{16–40}$), quartz, biotite, hornblende and augite are the major mineral phases found in the rocks, and zircon and apatite are the accessory minerals. Sericite, chlorite, epidote and clay minerals are found as secondary phases.

https://doi.org/10.1017/S001675682300033X Published online by Cambridge University Press

The quartz diorite samples include, in decreasing order of abundance, plagioclase, hornblende, quartz, orthoclase, biotite and opaque minerals (Table S1; Fig. 3). Biotite is added to above mentioned major phases in the granodiorites. The granite has quartz, orthoclase, plagioclase, hornblende, biotite and opaque minerals (Table S1; Fig. 3).

Hornblende is in euhedral and subhedral forms. Some of them show twinning and some others are slightly chloritized. Plagioclase has euhedral and subhedral forms and is slightly sericitized and partially fractured. It shows albite twinning and commonly presents ring zoning with sieve texture. Orthoclase occurs in the form of subhedral small crystals and shows in places Carlsbad twinning. Poikilitic and perthitic textures are observed in some orthoclase crystals. Small hornblende, plagioclase and opaque mineral inclusions are observed in areas where poikilitic texture is found. Orthoclase has altered into clay and sericite. Myrmekitic texture is seen between orthoclase and plagioclase. Quartz is found as large and small anhedral crystals. Quartz with subhedral orthoclase fills the gaps between the other minerals. Wavy extinction is observed in some quartz crystals. Biotite is in the form of euhedral to subhedral crystals and slightly altered into chlorite. Opaque minerals consist of magnetite and pyrite.

4.b. Mineral chemistry

The chemical compositions of the plagioclase, K-feldspar, amphibole, biotite and magnetite from the samples of the pluton are given in supplementary Table S2.

Plagioclase: Compositional zoning is, more or less, a ubiquitous feature of the plagioclases from the pluton. It is indicated by the variation of anorthite (An) end-member from 10.25 in the rim to 61.95 in the core (Fig. 4a). As shown by An–Ab–Or classification diagram (Smith & Brown, 1988), rim composition of the plagioclases is largely oligoclase and anorthite increase towards the core of the plagioclases generally reaches up to andesine and, to a very lesser extent, labradorite composition (Fig. 4a).

Orthoclase: In contrast to plagioclase, SiO_2 content of orthoclase does not display a large variation. A similar situation is valid for the Al_2O_3 and K_2O contents as well. All these show the absence of an important compositional zoning in orthoclase (Fig. 4a). The Or end-member of the orthoclase varies from Or_{93} in the cores to Or_{83} in the rims (Table S2).

Hornblende: Amphiboles display calcic composition (Ca+Na>1; 0>Na<0.5;) and plots in Mg-hornblende and actinolite fields in the amphibole classification diagram of Leake *et al.* (1997) (Fig. 4b). The rims of amphiboles show actinolite composition. Si and Al^t contents of hornblende increase together. The MnO and TiO_2 contents of hornblende vary from 0.27 to 1.08 wt% and 0.10 to 2.03 wt%, respectively, and $Mg/(Mg+Fe^{2+})$ ratios between 0.56 and 0.76. Hornblende generally contains low F (0.19 to 0.55 wt%) and Cl (0.02 to 0.29 wt%), indicating that there is no volatile enrichment during its formation.

Biotite: $Fe^{+2}/(Fe^{+2}+Mg)$ and $Mg/(Mg+Fe^{2+})$ ratios of biotite are between 0.39 and 0.49, and 0.51 and 0.61, respectively. Biotite is the product of solid solution series between phlogopite and annite end-members and has 60% phlogopite and 40% annite that is slightly closer to the magnesium-rich phlogopite end (Fig. 4c).

Magnetite-ilmenite: Magnetite contains 0.06 to 0.34 wt% of TiO_2 and 91.42 to 93.27 wt% of FeO^t, and same major oxide contents in ilmenite vary from 46.97 to 48.27 wt% and 45.44 to 48.04 wt%, respectively (Table S2). Magnetite is the product of ulvospinel-magnetite solid melt, and mostly has compositions close to the magnetite end (Fig. 4f). Ilmenite is located between ilmenite and hematite.

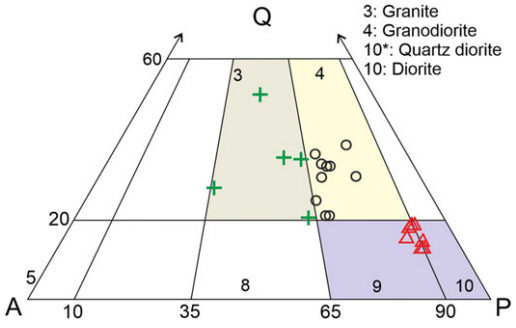

Figure 3. (Colour online) QAP diagram (modified from Streckeisen, 1976) for the modally analyzed samples of the pluton.

4.c. U–Pb zircon geochronology

In order to determine the timing of magma emplacement and constrain its crystallization age, U–Pb zircon SHRIMP dating was performed on two granodiorite samples (Tables S3). Zircons are generally small to moderate crystals varying in size between 70 and 310 μm (Fig. 5a). They are commonly elongated grains, mostly euhedral to subhedral in shape and partly fractured. The compositional zoning is a common feature of the zircon grains, indicating that zircon minerals are of magmatic origin. Xenocrystic core is rarely observed. Zircon grains from the sample C1 have Th/U ratios in the range of 0.57 to 1.29 (Table S3). The minimum $^{206}Pb/^{238}U$ (1σ) age is 42.7 ± 1 Ma and the highest $^{206}Pb/^{238}U$ (1σ) age is 48.0 ± 2 Ma (Fig. 5a and b). The weighted average (concordia) age is 44.75 ± 0.92 Ma (MSWD = 1.2) for the sample C1 and 45.01 ± 0.59 Ma (MSWD = 2.0) for the sample C4, which correspond to the Lutetian (Eocene) and is interpreted as the intrusion age of the pluton (Fig. 5b).

4.d. Geochemistry

4.d.1. Major, trace and REEs

Geochemical compositions of the analyzed samples are presented in supplementary Table S4. Similar to the distribution shown in the modal QAP diagram, the samples have a wide compositional range from diorite to granite in the classification diagram of Middlemost (1994) (Fig. 6a). Samples fall in the field of rocks with magnesian affinity in the diagram of Frost *et al.* (2001).

The samples with ASI [molar $Al_2O_3/(CaO+Na_2O+K_2O)$] values lower than 1 are metaluminous in character (Fig. 6d). They present a high K calc-alkaline composition in the K_2O-SiO_2 diagram (Le Maitre, 1989).

Major oxides and some trace elements versus SiO_2 diagrams show almost linear covariations (Fig. 7), suggesting that fractional crystallization (FC) is an effective tool in the development of compositional range in the pluton. Negative correlations of CaO, MgO, Al_2O_3, Fe_2O_{3t}, TiO_2 and P_2O_5 against SiO_2 are distinct, whereas K_2O and Na_2O display positive relationships. Trace elements, except for Sr, also generally show an obvious positive correlation against SiO_2. The scattered distribution observed in Ni may be partially related to weathering, contamination or magma mixture.

In the primitive mantle-normalized multi-element diagram (Fig. 8a), the samples of the Dağdibi Pluton present enrichments of large ion lithophile elements (LILE) such as Rb, Ba and Th

https://doi.org/10.1017/S001675682300033X Published online by Cambridge University Press

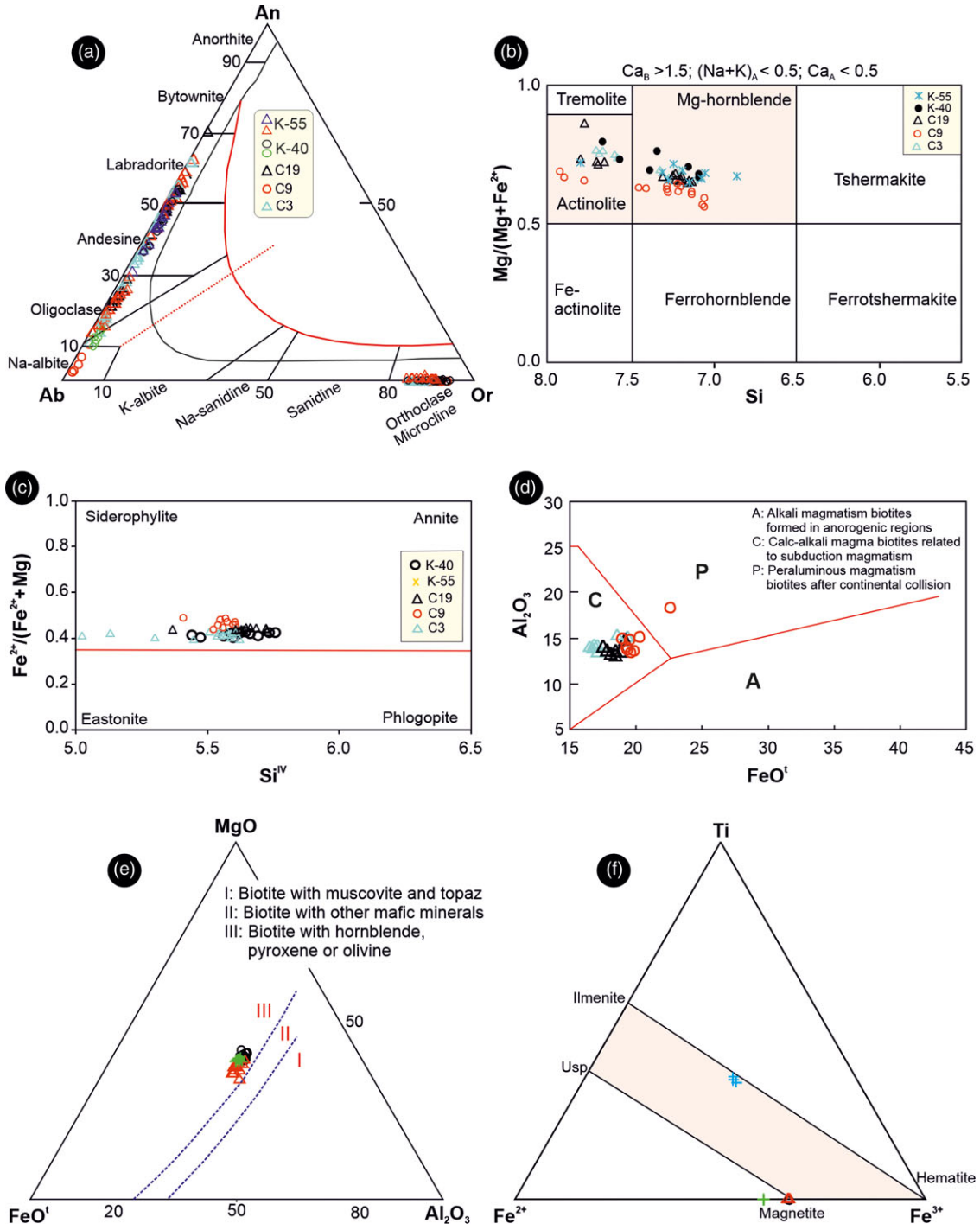

Figure 4. (Colour online) (a) The An–Ab–Or classification diagram for the feldspars of the pluton (modified from Smith & Brown, 1988; data of K-55 and K-40 from Sipahi *et al.* 2018b). (b) Classification of amphiboles from the pluton (modified from Leake *et al.* 1997; data of K-55 and K-40 from Sipahi *et al.* 2018b). (c) Si vs $Fe^{2+}/(Fe^{2+}+Mg)$ diagram for biotites. (d) Al_2O_3-$FeO^{(t)}$ for biotites (symbols are same as Fig. 4c). (e) MgO–$FeO^{(t)}$ –Al_2O_3 diagram for biotite (modified from Speer, 1987; symbols are same as Fig. 4c). (f) Ti–Fe^{2+}–Fe^{3+} diagram for magnetite and ilmenite minerals (modified from Bacon & Hirschmann, 1988).

generally over 100 times relative to high field strength elements (HFSE). Negative anomalies in Nb, P and Ti, and a positive anomalies in Pb are quite pronounced (Fig. 8a), which are typical for those formed in subduction and post-collisional settings with protoliths metasomatized via the addition of solutions during the previous subduction.

REE distributions of the samples normalized to chondrite (Boynton, 1984) are shown in Fig. 8b. Light rare earth elements (LREE) are more enriched in the granodiorite samples than those of the others. The LREEs are generally moderately fractionated compared to HREEs (La_N/Lu_N = 4.12–7.90) and samples have moderate to strong negative Eu anomalies (Eu/Eu * = 0.55–0.82) (Fig. 8b).

4.d.2. Sr, Nd and Pb isotope geochemistry

Mean age of 45 Ma was used for the calculations of $^{87}Sr/^{86}Sr_{(i)}$, $\epsilon Nd_{(i)}$ values, and Nd depleted mantle model ages (T_{DM}^{1} and T_{DM}^{2};

https://doi.org/10.1017/S001675682300033X Published online by Cambridge University Press

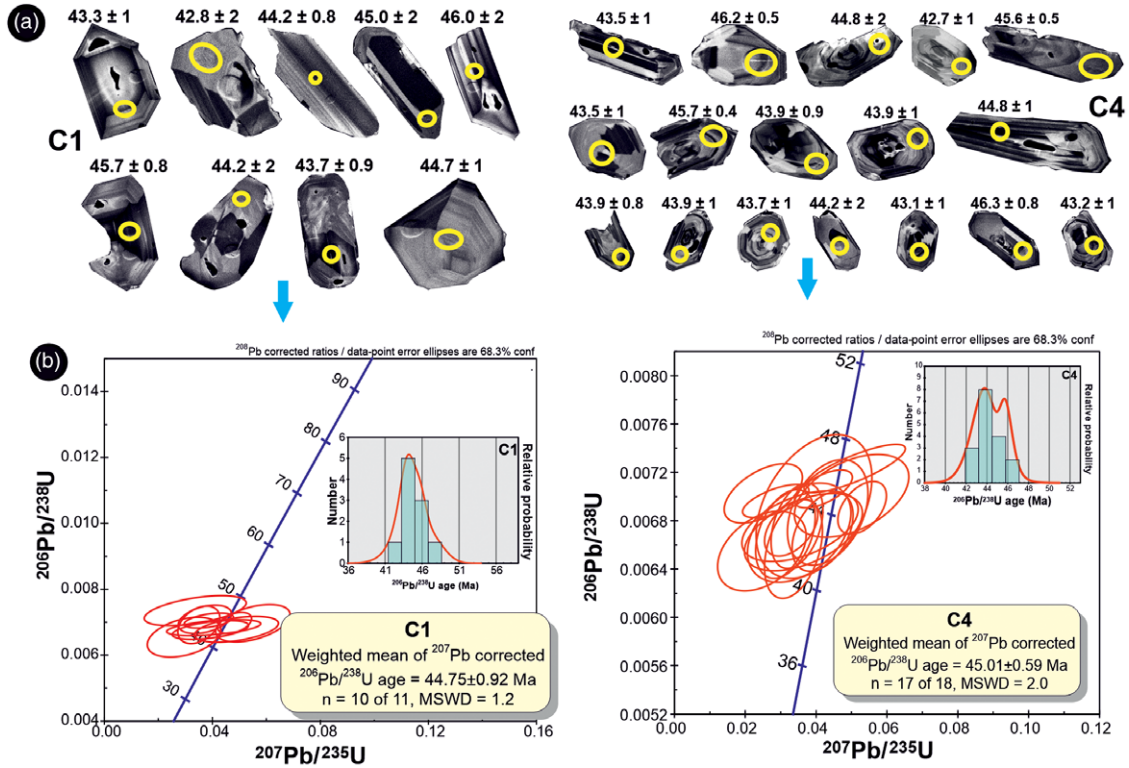

Figure 5. (Colour online) Selected zircon crystals from the granodiorite samples C1 and C4. (a) cathodoluminescence (CL) images of zircon crystals and the location of analyzed spots and (b) $^{206}Pb/^{238}U$–$^{207}Pb/^{235}U$ Wetherill Concordia diagrams with insets of probability distribution-age diagrams.

Table S5). $^{87}Sr/^{86}Sr_{(i)}$ ratios and $\epsilon Nd_{(45Ma)}$ values vary in narrow ranges from 0.704845 to 0.705726 and –1.42 to +0.08, respectively.

In the $\epsilon Nd_{(45Ma)}$-$^{87}Sr/^{86}Sr_{(45Ma)}$ diagram, all the analysed samples are grouped in the mantle array close to the bulk silicate Earth except for a sample plotting just outside the mantle array (Fig. 9a). Also shown on the plot are the fields of other plutonic rocks from the same region for comparison. The Dağdibi samples have lesser radiogenic isotope ratios compared to those of the Late Cretaceous and middle Eocene granitic rocks.

Pb isotope ratios of the rocks vary between 18.206 and 18.621 for $^{206}Pb/^{204}Pb_{(i)}$, 15.590 and 15.628 for $^{207}Pb/^{204}Pb_{(i)}$ and 37.743 and 39.520 for $^{208}Pb/^{204}Pb_{(i)}$ (Table S5). While the isotope ratios of the $^{206}Pb/^{204}Pb_{(i)}$ and $^{207}Pb/^{204}Pb_{(i)}$ are distributed in a narrow range, the $^{208}Pb/^{204}Pb_{(i)}$ isotope ratios exhibit a wide distribution. A positive correlation is observed in the isotope diagrams of $^{206}Pb/^{204}Pb_{(i)}$ versus $^{207}Pb/^{204}Pb_{(i)}$ and $^{208}Pb/^{204}Pb_{(i)}$ of the samples (Fig. 9b and c). The Dağdibi samples fall in the field of lower crust and the upper part of the Northern Hemisphere Reference Line (NHRL). In addition, all the samples are located between the Enriched Mantle I (EM I) and Enriched Mantle II (EM II) fields and plot closer to the field of EM II reservoir (Fig. 9b and c). The samples of the Dağdibi Pluton have Pb isotope ratios resembling characteristically those of the lower crust (Fig. 9b) as observed in the other middle Eocene plutons in the region such as Eğrikar and Karadağ (Sipahi *et al.* 2018b).

4.d.3. Hf isotope geochemistry

The Lu–Hf isotopes of the zircons were determined to make estimations on the possible mantle source(s) of the studied rocks. $\epsilon Hf_{(i)}$ values of zircons from the granodiorite samples range from +0.14 to +10.26 (Table S6). The $^{176}Hf/^{177}Hf_{(i)}$ ratios of the studied zircons plot on the depleted mantle (DM) line (Fig. 10a). The $\epsilon Hf_{(i)}$ values show a narrow range and plot between depleted mantle and chondrite uniform reservoir (CHUR) lines (Fig. 10b and c). The Hf isotopes of the zircons yield TDM_1 (single-stage Hf isotope) model ages of 0.277 to 0.623 Ma (Table S6) and offer a uniform property, suggesting derivation from the same source for the Middle Eocene magmatism.

4.d.4. Temperature and pressure

The amphibole-plagioclase thermometer: $T = 0.667\ P – 48.98 + Y/– 0.0429 – 0.008314\ LnK$, is an empirical formula proposed by Blundy & Holland (1990), is widely used to calculate the crystallization temperature of magmas. Here, pressure (P) is calculated from amphibole minerals that developed in contact with each other at equilibrium crystallization. For $X_{ab} < 0.5$, $Y = -8.06 + 25.5(1-X_{ab})^2$ is used. If $X_{ab} > 0.5$, then $Y=0$. The K value with the formula $(Si-4/8-Si)X_{ab}$ is a special number. Requirements for using this thermometer are that amphibole–plagioclase equilibrium crystallization should be accompanied by biotite, quartz, K-feldspar, pyroxene, Fe–Ti oxides ± sphene minerals and plagioclase should have a less calcic character than An_{92}. Additionally, the Si cationic value of the amphibole developing in contact with plagioclase should be lower than 7.8. The temperatures calculated for the rocks of the pluton range between 625 and 744 °C (Table S7) for granodiorite, 662 °C for diorite.

A formula proposed by Luhr *et al.* (1984) for *biotite thermometer* was also used to check the crystallization temperatures. The biotite crystallization temperatures for the investigated plutonic rocks are in the range of 627–762°C for granodiorite and 735–781 °C for diorite (Table S8), consistent with those of amphibole–plagioclase thermometer.

https://doi.org/10.1017/S001675682300033X Published online by Cambridge University Press

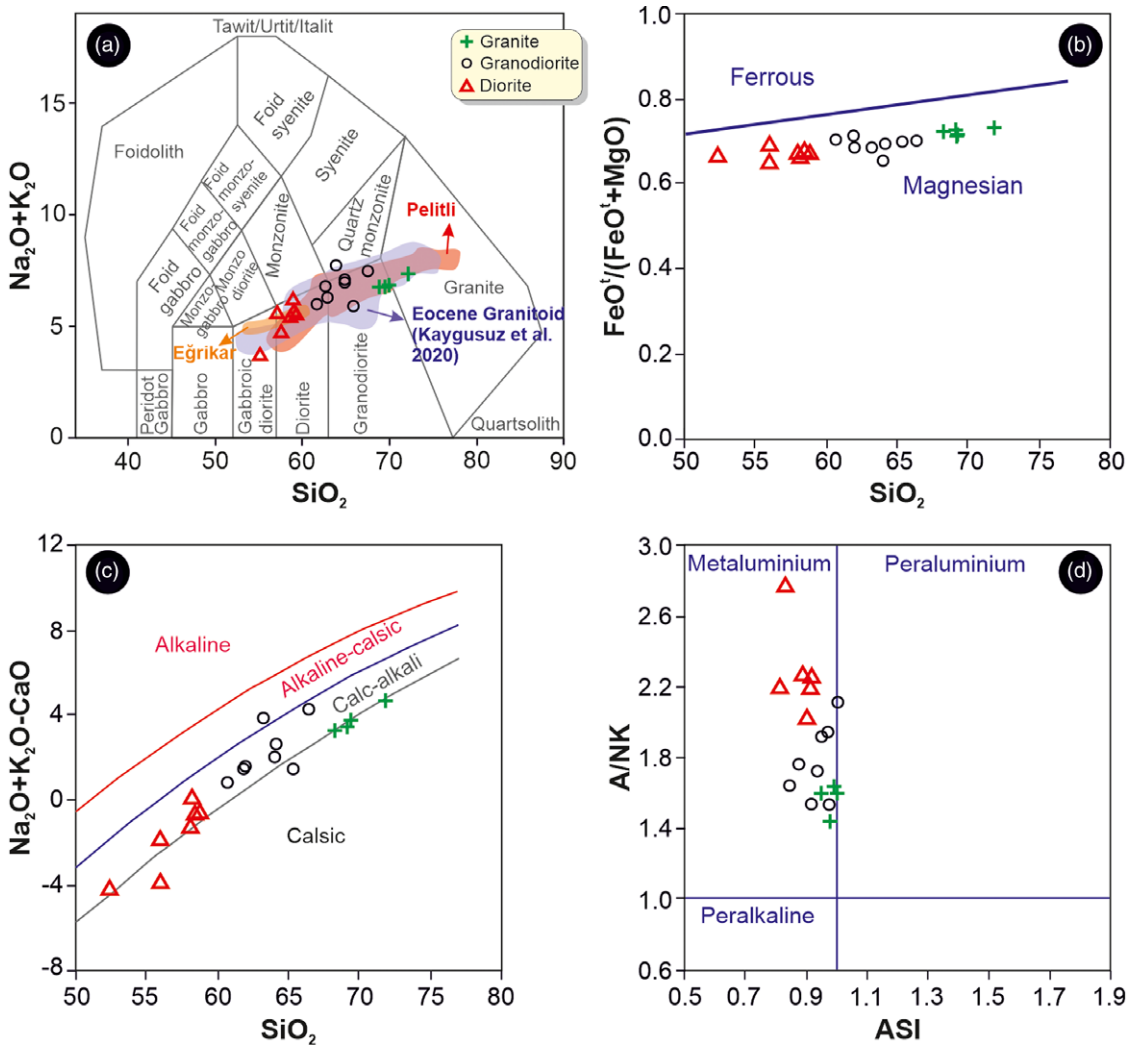

Figure 6. (Colour online) Chemical classification diagrams. (a) SiO_2 vs Na_2O+K_2O diagram (Middlemost *et al.* 1985), (b) SiO_2 vs (FeO^t/FeO^t+MgO), c) SiO_2 vs (Na_2O+K_2O+CaO) and d) ASI vs A/NK diagram (Frost *et al.* 2001).

Ilmenite–magnetite thermometer: The ILMAT program (Lepage, 2003) was used to calculate the temperature and oxygen fugacity values for the studied rocks. The approaches suggested by Spencer & Lindsley (1981) and Andersen & Lindsley (1985) were used to calculate the temperature values. The chemical compositions of magnetite and ilmenite give the mean crystallization temperatures in the range from 561 to 583 °C according to Spencer & Lindsley (1981)' and from 567 to 591 °C according to Andersen & Lindsley (1985) (Table S9). The oxygen fugacity values are in the range of −18.35 to −17.04 for the diorites.

Zircon and apatite saturation temperatures calculated from whole-rock geochemical analysis of rock samples (Watson & Harrison, 1983; Hanchar & Watson, 2003; Miller *et al.* 2003) range from 767 to 802 °C and 886 to 900 °C for granite, 744 to 797 °C and 857 to 890 °C for granodiorite, 699 to 753 °C and 740 to 852 °C for diorite, respectively (Table S10).

The amphibole geothermometer and geobarometer: Crystallization temperature of magma is calculated by using the Si in amphibole (Mg hornblende in this study) according to the formula (T (°C) = −151.487 × Si* + 2041) of Ridolfi *et al.* (2010) (Table S11). The amphibole compositions of samples yield the crystallization temperatures in the range of 691 to 792 °C for the Dağdibi Pluton. There is a linear relationship between the total aluminium content of amphiboles and increasing pressure and temperature (Hammarstrom & Zen, 1986; Hollister *et al.* 1987; Johnson & Rutherford, 1989; Schmidt, 1992). $Al^{(T)}$ in hornblende crystallized in granitoid magmas is known as the pressure indicator and used for pressure calculations with various calibrations. The pressure values of amphiboles, whose sub-species are determined as actinolite and Mg–hornblende, were calculated according to the Al–hornblende geobarometer of Hammarstrom & Zen (1986), Hollister *et al.* (1987), Johnson & Rutherford (1989), Schmidt (1992) and Mutch *et al.* (2016), but in this study the pressure values calculated from Mg–hornblende were preferred (Table S11). The pressure conditions during the crystallization of amphiboles vary between 0.38 and 2.45 kbar according to Schmidt (1992) and 0.97 and 2.19 kbar according to Mutch *et al.* (2016). The cooling depth (1 kbar = 2.7 km) corresponding to these pressures ranges from 2.6 to 5.9 km. The negative and very low-pressure values of amphiboles are interpreted as the effect of alteration and a low degree of metamorphism and so were not used. Al content in Ca-amphiboles increases with increasing degree of metamorphism (Leake, 1964; Graham, 1974). The calculated pressures and temperatures of amphiboles from the Dağdibi Pluton show a linear relationship.

https://doi.org/10.1017/S001675682300033X Published online by Cambridge University Press

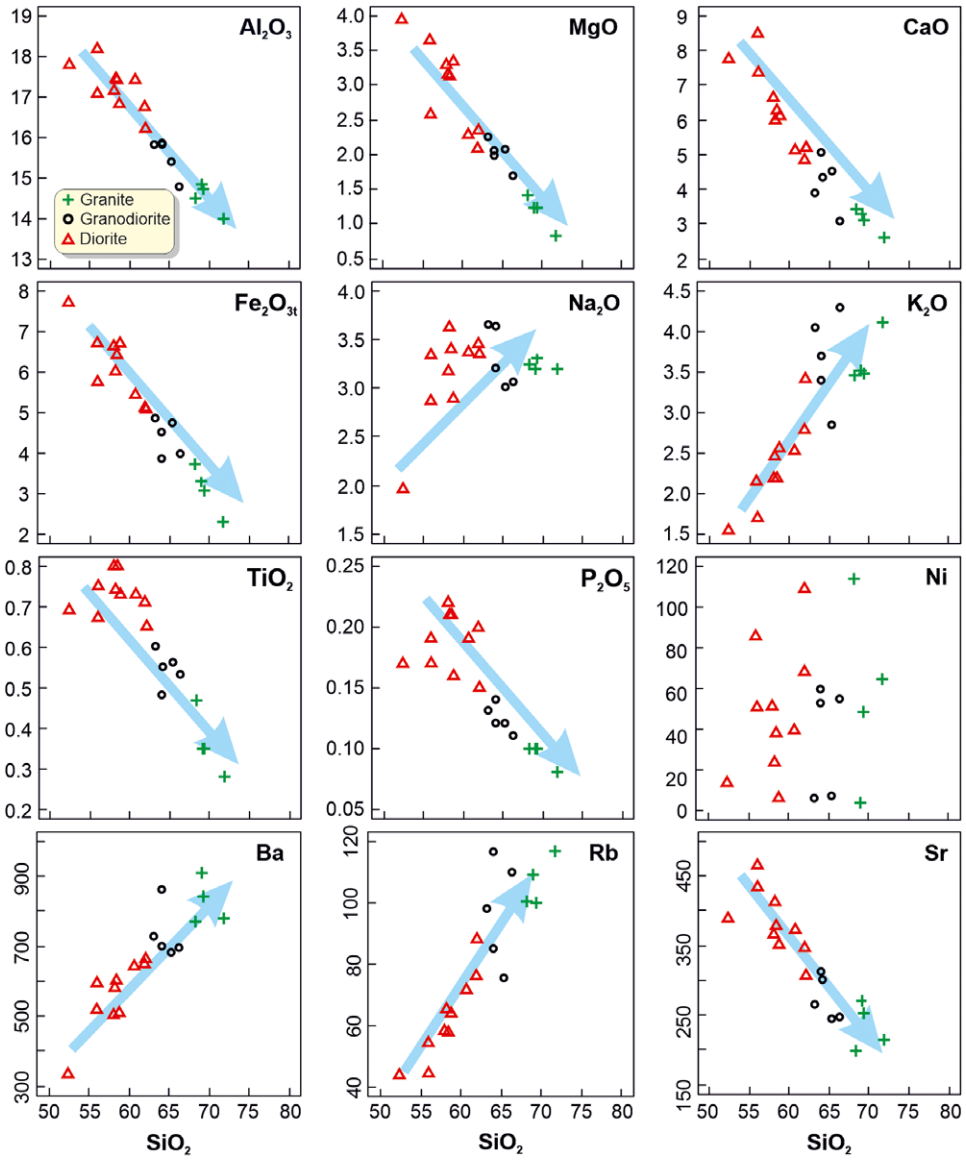

Figure 7. (Colour online) SiO_2 content of pluton versus CaO, MgO, Al_2O_3, $Fe_2O_3^t$, TiO_2, Na_2O, K_2O and P_2O_5. and trace (Ba, Rb, Sr and Ni) element contents distributions.

5. Discussion

5.a. Age of the pluton

Igneous activity that occurred in a time interval from the Late Cretaceous to the end of the Eocene occupies the largest area in the eastern Sakarya Zone (Fig. 1a). Considering that the region had a magmatic arc position in the Late Cretaceous and evolved into a syn to post-collisional setting in the Eocene, precise determination of the ages of the igneous rocks is of great importance. This discrimination becomes much more important when considering that the Late Cretaceous plutonic bodies were intruded later by magmas of the middle Eocene plutonic bodies in the inner-arc setting (Dokuz *et al.* 2019).

U–Pb zircon ages of 44.75 ± 0.92 and 45.01 ± 0.59 Ma refer the intrusion age of the parental magma for the Dağdibi Pluton to the middle Eocene. So, it is one of the numerous members of the post-collisional plutonic bodies of middle Eocene age in the eastern Sakarya Zone. The Sisdağı Pluton (41 Ma, Karslı *et al.* 2012), Erik Granitoid (42 Ma, Sipahi *et al.* 2017), Kaletaş Pluton (44 Ma; Arslan & Aslan, 2006), Karadağ Diorite (44 Ma, Sipahi *et al.* 2022) and Bayburt Plutons (44–45 Ma; Eyüboğlu *et al.* 2017) are some other examples of this group in the surrounding region. Interestingly, while the Eocene magmatic activity in northwest Anatolia is mostly between 54 and 45 Ma (Okay *et al.* 2022), there is a significant number of the plutonic activities in the Sakarya Zone ranging in age predominantly from 46 to 36 Ma (Fig. 11).

5.b. Mineral chemistry

Mg-rich biotite is rather known as the product of water-saturated magmatic systems (Patiño Douce & Johnston, 1991). The water in the system is supplied by the dehydration of the subducted material, and some of the Fe in the environment is used in the amphibole and Fe–Ti oxide is formed with the other Fe amount. The chemical composition of Mg-rich biotite implies that the pluton might have been formed from a water-saturated calc-alkaline magma in subduction-related setting.

Biotites crystallizing in calc-alkali, alkali and peraluminous granitic magmas differ significantly in their Al_2O_3, FeO^t and MgO contents and therefore provide important information about the

https://doi.org/10.1017/S001675682300033X Published online by Cambridge University Press

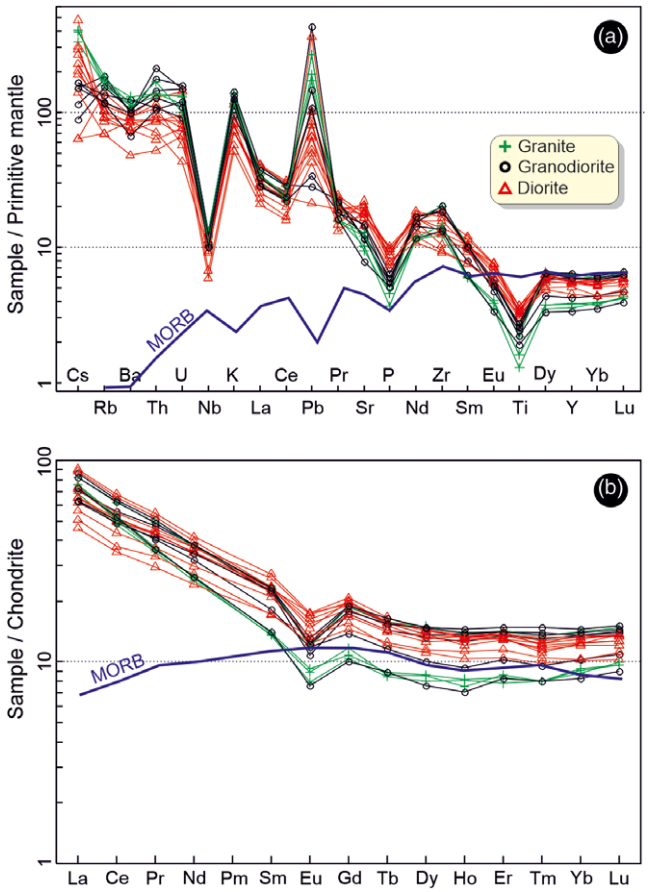

Figure 8. (Colour online) (a) Primitive mantle-normalized multielement diagram for the studied samples of the Dağdibi Pluton (Sun & McDonough, 1989) and (b) chondrite-normalized REE diagram for the samples (Boynton, 1984).

tectonic settings of magmas (Abdel-Fattah, 1994). When biotites are put to the Al_2O_3-FeO^t discrimination diagram, they have grouped in the field of subduction-related magmas (Fig. 4d; Abdel-Fattah, 1994).

FeO^t/MgO ratio of biotite crystallizing in anorogenic-alkaline magmas (forming A-type granites) is on average 7.04. While FeO^t/MgO ratio in biotite crystallizing from the peraluminous magmas (S-type granites) is 3.48, this ratio of biotite in the calc-alkaline magmas (I-type granites) of orogenic belts decreases to 1.76 with the increasing Mg in biotite. The FeO^t/MgO ratio in the studied biotite minerals ranges from 1.70 to 1.18, indicating that the biotite minerals were developed in I-type granitoid magmas with calc-alkaline nature in subduction-related setting. The compositions of biotites plot in the field III in the MgO-FeO^t-Al_2O_3 triangle diagram (Speer, 1987) where it is found with "hornblende, pyroxene, or olivine" (Fig. 4e).

5.c. Thermometer, pressure and oxygen fugacity

The temperature values obtained for the rocks of the Dağdibi Pluton are similar to those found in the Dölek, Sarıçiçek, Sorkunlu, Üzengili and Arslandede plutons (388–1196 °C, Eyüboğlu *et al.* 2017).

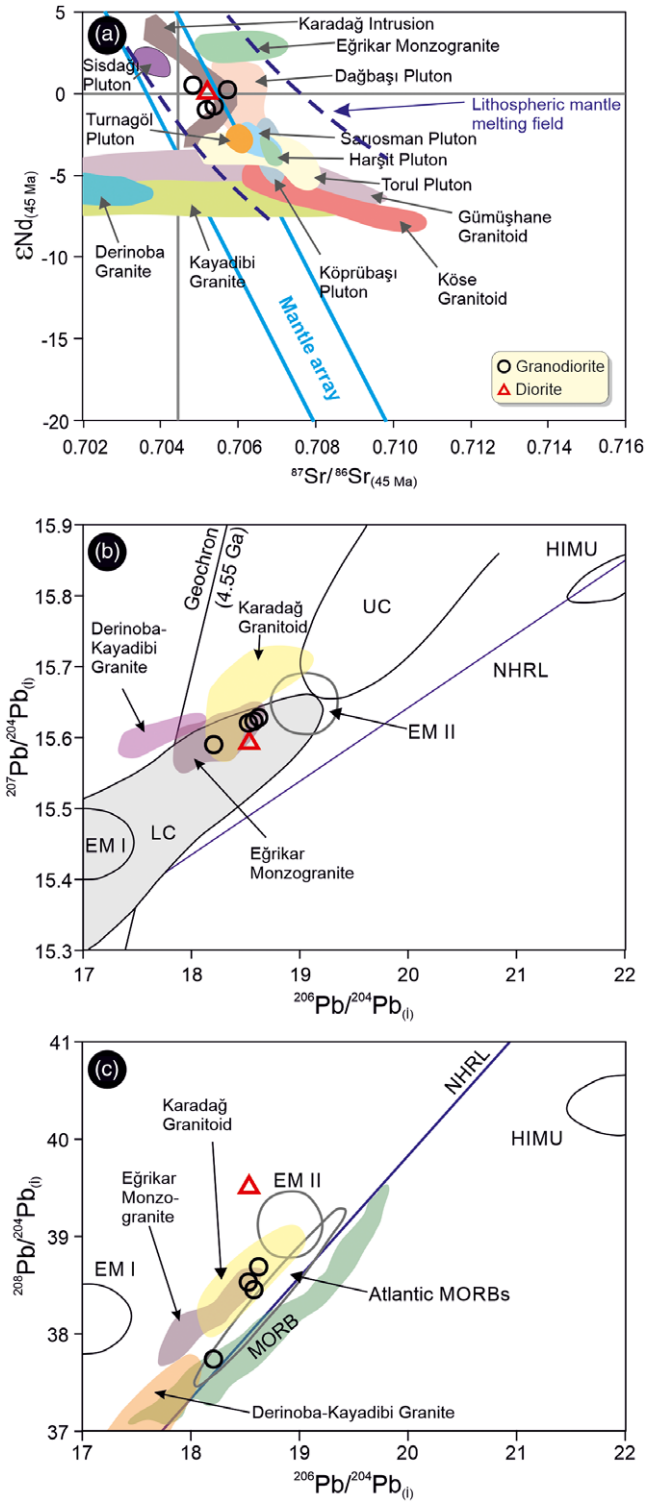

Figure 9. (Colour online) Distributions of the Dağdibi samples in the isotope correlation diagrams. (a) $\epsilon Nd_{(45Ma)}$–$^{87}Sr/^{86}Sr_{(45Ma)}$ isotope correlation and age taken as 45 Ma, (b) $^{206}Pb/^{204}Pb_{(i)}$ vs $^{207}Pb/^{204}Pb_{(i)}$ and (c) $^{206}Pb/^{204}Pb_{(i)}$ vs $^{208}Pb/^{204}Pb_{(i)}$ isotope diagrams. NHRL: North Hemisphere Reference Line (Hart, 1984); EMI and EMII: Enrichment Mantle I and II (Zindler & Hart, 1986); LC: lower crust (Kempton *et al.* 1997); UC: upper crust (Mason *et al.* 1996); HIMU: high μ mantle (Zindler & Hart, 1986); Atlantic MORBs: Atlantic middle ocean rift basalt. Derinoba and Kayadibi Granites (Kaygusuz *et al.* 2012), Eğrikar Monzogranite (Sipahi *et al.* 2018a), Karadağ Intrusion (Sipahi *et al.* 2022).

https://doi.org/10.1017/S001675682300033X Published online by Cambridge University Press

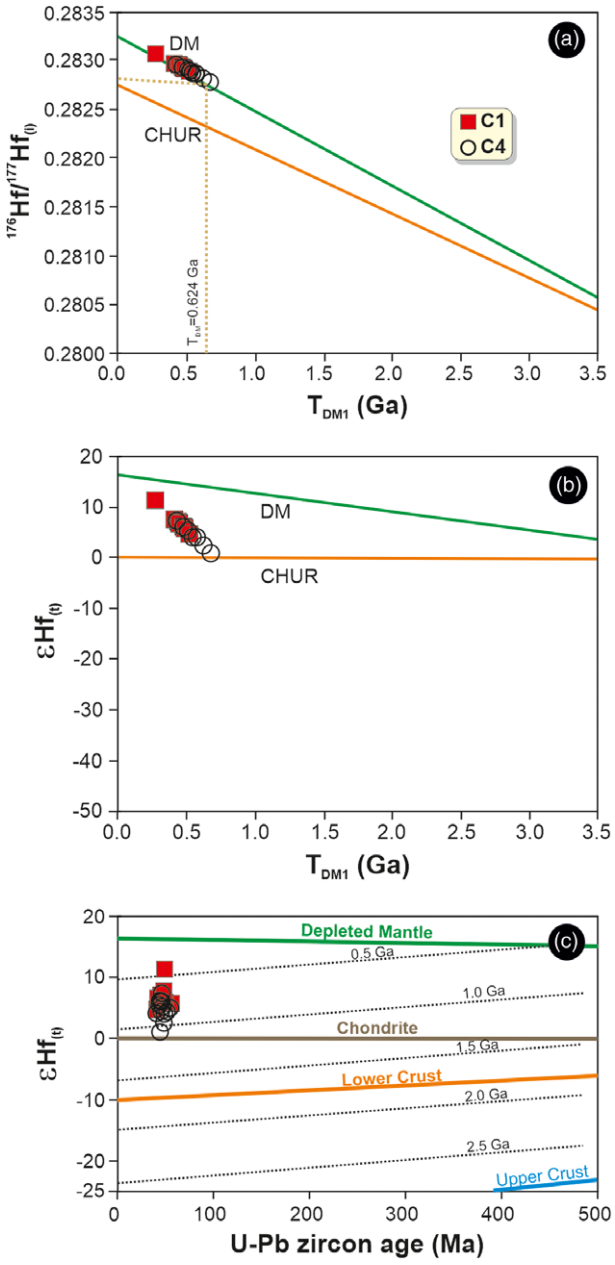

Figure 10. (Colour online) (a) $^{176}Hf/^{177}Hf_{(i)}$ vs $T_{DM1(t)}$ (Ga), (b) $\epsilon Hf_{(t)}$ vs $T_{DM1(t)}$ (Ga), c) $\epsilon Hf_{(t)}$ vs U–Pb zircon age (Ma) from the granodiorite samples.

Amphibole-plagioclase barometer yields pressure values for the Dağdibi Pluton similar to those of other Eocene plutons from Bayburt (0.1 to 2.2 kbar, Kaygusuz *et al.* 2018), but lower than those of the Dölek-Sarıçiçek-Üzengil-Arslandede plutons (0.3 to 8.2 kbar, Eyüboğlu *et al.* 2017). The crystallization depths (1 kbar = 2.7 km) estimated from the calculated pressure values of the amphiboles correspond to some places between 3 and 6 km in the upper crust.

Since the original oxygen fugacity of granitic magmas cannot be determined precisely due to slow cooling, only the relative approaches and calculations can be provided (Anderson & Smith, 1995; Kemp, 2004). Oxygen fugacity ($\log_{10} fO_2$) values of the Dağdibi Pluton are in the range of −18 to −17 similar to those found in the Eocene Dölek-Sarıçiçek plutons (−15 to −21) and a granitoid body (−20 to −12) from Bayburt (Kaygusuz *et al.* 2018).

There is no consensus on the water content of amphibole-containing magmas. It varies from 2 to 3 wt% according to Luhr (1992) and is around 6 wt% on average, according to Merzbacher & Eggler (1984). Calculated H_2O values of the amphibole in this study change from 1.68 to 4.17 wt%. The presence of hydrous mafic minerals (amphibole and biotite) and apatite in samples points to high water and volatile content of magma. If the temperature of magma is so high with such a high-water content, it can rise to the shallow depths of the continental crust without crystallizing completely (Helmy *et al.* 2004).

5.d. Petrogenesis of the Pluton

The Dağdibi Pluton has high K-calk-alkaline (Fig. 6c) and metaluminous (ASI<1) character. Two models have been proposed regarding the origins of high-K calc-alkaline magmas. These are (1) partial melting of basic lower crustal rocks at relatively high pressure (Roberts & Clemens, 1993) and (2) mixture of magmas derived from crustal and mantle sources (Barbarin, 1999).

The samples of the pluton display weak to moderate REE fractionations ($(La/Yb)_N = 5.90$ to 21.31) in chondrite-normalized diagram, low Sr/Y ratios (6.67 to 24.16) and high *Y* (13.7 to 30.1 ppm) and Yb (1.48 to 3.29 ppm) contents. The rocks of the pluton display high-K calc-alkaline and I-type character and have relatively low Ni (1.6 to 113.9 ppm) contents with relatively low Mg-numbers (22–44) and a wide range of silica content ($SiO_2 = 52.36$ to 71.81 wt%). The samples show enrichment in large ion lithophile (LIL) elements, negative Nb and Ta anomalies and positive Pb anomalies. Negative anomalies in Nb, P and Ti are the typical features of subduction-related magmas. Abundance of large ion lithophile elements in the mantle is usually revealed by the additions of solutions from the subducted slab (McCulloch & Gamble, 1991). All these data indicate that the rocks were formed by the mixing of melts derived from lower crust (amphibolitic) and lithospheric mantle sources.

5.d.1. Fractional crystallization and assimilation

The positive and negative trends of some major and trace elements with the increasing SiO_2 imply that FC has played an important role during the development of the pluton. High CaO and Sr contents and slightly negative Sr and Eu anomalies indicate plagioclase fractionation. The trends in the Rb/Sr versus Sr and Ba/Sr versus Sr diagrams suggest that plagioclase differentiation has played an important role in the formation of the present composition of the rocks (Fig. 12). The negative trends in Al_2O_3, MgO, CaO, Fe_2O_{3t} values against SiO_2 and the increase in K_2O and Ba contents can be attributed to amphibole and calcic plagioclase fractionation. The increase in K_2O and Rb with increasing SiO_2 indicates that they are the products of accumulation rather than fractionation of K-feldspar and biotite. The decrease in P_2O_5 and TiO_2 contents with increasing SiO_2 indicates apatite and titanite differentiation. The increase in Y and Zr indicates the accumulation of accessory minerals such as zircon and titanite.

The most felsic granite specimen of the pluton has a high content of SiO_2 (71wt%pri) and a low Mg-number (24), supporting that the mineral fractionation is an important process for the formation of felsic rocks. The most primitive sample has 52 wt% SiO_2 and a Mg-number value of 31. If the primitive rocks of the pluton had been formed by direct partial melting of mantle peridotites, the Mg# values of the samples should have been higher

https://doi.org/10.1017/S001675682300033X Published online by Cambridge University Press

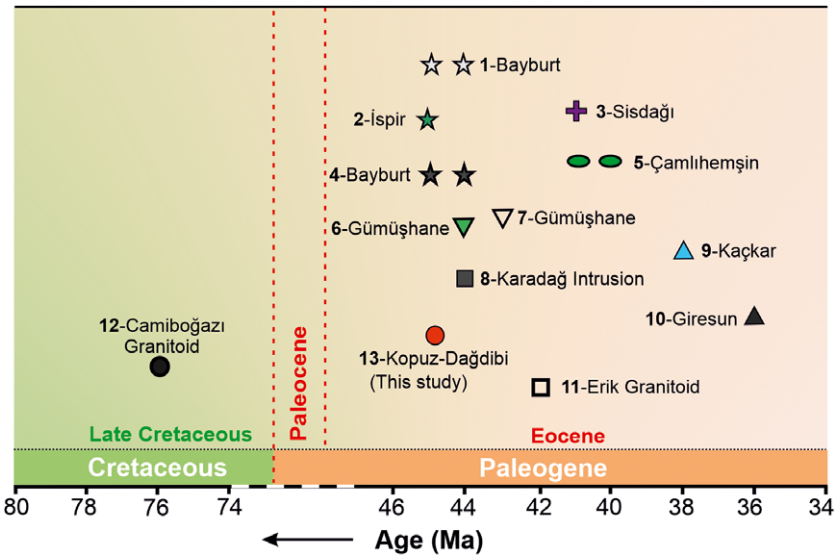

Figure 11. (Colour online) The U–Pb zircon ages of the Eocene plutons from the eastern Sakarya Zone. 1-Bayburt: Kaygusuz *et al.* (2018, 2020); 2-İspir: Dokuz *et al.* (2019); 3-Sisdağı: Karslı *et al.* (2012); 4-Bayburt: Eyüboğlu *et al.* (2017); 5-Çamlıhemşin: Dokuz *et al.* (2019); 6-Gümüşhane: Arslan & Aslan (2006); 7-Gümüşhane: JICA (1986); 8-Karadağ Intrusion: Sipahi *et al.* (2018b); 9-Kaçkar: Boztuğ *et al.* (2007); 10-Giresun: Boztuğ *et al.* (2004); 11-Erik Granitoid: Sipahi *et al.* (2017); 12-Camiboğazı Granitoid: Kaygusuz *et al.* (2014); 13-Kopuz-Dağdibi: this study.

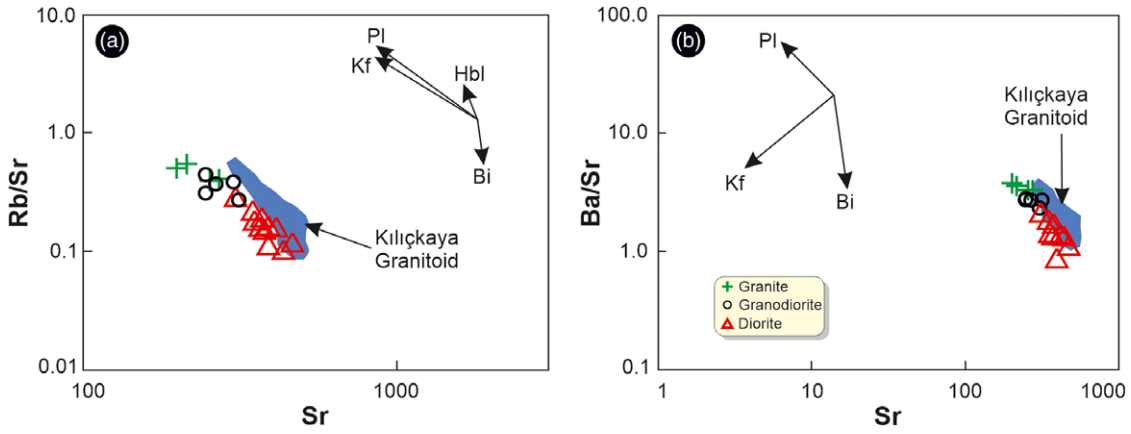

Figure 12. (Colour online) Distributions of the samples in (a) Rb/Sr vs. Sr and (b) Ba/Sr vs. Sr diagrams. Kılıçkaya Granitoid (Kaygusuz & Öztürk, 2015).

than 65. Linear elemental variations (Fig. 7) along with low SiO_2 values suggest that even the primitive rocks of the pluton might have been formed by crystal fractionation from a more primitive basaltic magma. An alternative way to produce such high-K calc-alkaline andesitic magmas is that they may have formed through high degree of partial melting of calc-alkaline mafic crustal rocks at lower crust (Roberts & Clemens, 1993).

The negative Nb (Ta) and positive Pb anomalies (Fig. 8) point to subduction influence on the rocks and/or crustal contamination. Such depleted Nb values and other high-field strength elements may have also resulted from crustal contamination. This inference is consistent with the high Th (4.4 to 18 ppm) and Pb (1.5 to 30.6 ppm) contents of the samples that imply the contributions of crustal contamination since the crustal components are rich in Th (3.5 ppm) and Pb (8 ppm) (Taylor & McLennan, 1985). The $^{87}Sr/^{86}Sr_{(i)}$ ratios, on the other hand, are nearly constant against increasing SiO_2, indicating that FC played a greater role than crustal contamination during the evolution of the Dağdibi Pluton.

5.d.2. Magma mixing

Some researchers (e.g, Grove & Donelly-Nolan, 1986; Hildreth & Moorbath, 1988) suggest that I-type granitoids are generally resulted from the interaction of basaltic magma with crustal components via assimilation-fractional crystallization (AFC) or have formed by magma mixing. Nevertheless, some other researchers (Chappell & White, 1992; Rapela & Pankhurst, 1996) have pointed out that relatively high siliceous magmas could have formed as a result of the FC of magmas derived from the lower crust. The presence of some disequilibrium textures (prismatic-cellular plagioclase growth, K-feldspars with poikilitic texture, etc.) in the rocks implies that interaction of two magmas with different chemical compositions have also played some role during the development of these rocks (Fig. 3). This inference is also confirmed by the presence of mafic microgranular enclaves.

Curvilinear relationships between trace element ratios are also a feature of rocks formed as a result of magma mixing (Perugini & Poli, 2004). The curvilinear trends shown in the Rb/Sr versus Ti/Zr and the Sr/Rb versus Sr diagrams (Fig. 13a and b) also imply the contribution of mixing of two different end-member components during the generation of the pluton.

5.e. Magma source

Low SiO_2 (52 wt%) contents, calc-alkaline and I-type characteristics of the less fractionated rocks point to the involvement of metaigneous rocks as the source in the crust or lithospheric mantle.

https://doi.org/10.1017/S001675682300033X Published online by Cambridge University Press

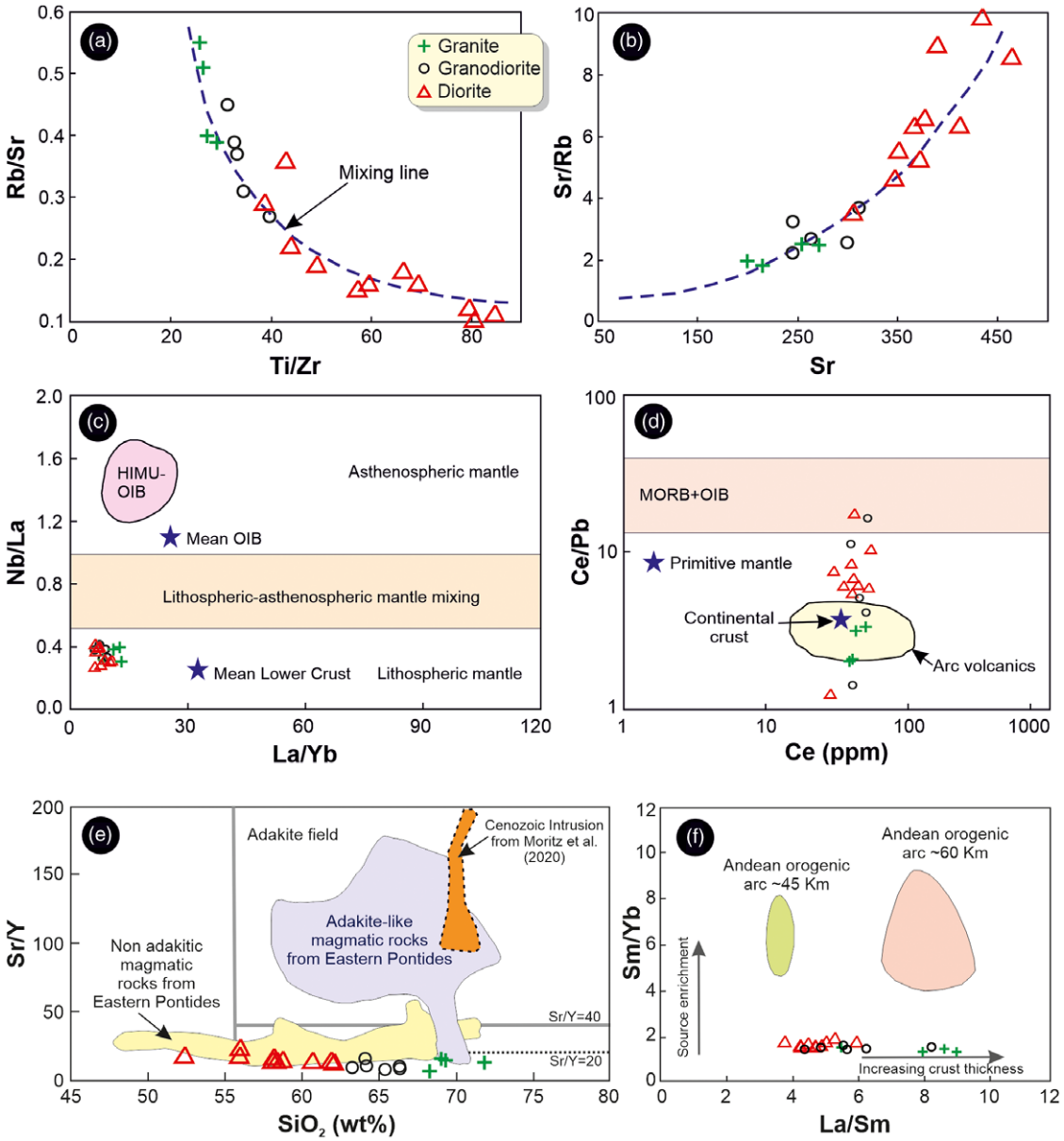

Figure 13. (Colour online) Distributions of the samples in various bivariation diagrams. (a) Rb/Sr vs Ti/Zr diagram, (b) Sr/Rb-Sr diagram of granitoid samples, (c) Nb/La vs La/Yb diagram, (d) Ce/Pb vs Ce diagram, (e) SiO_2 vs Sr/Y discrimination diagram (Moritz *et al.* 2020) and (f) La/Sm vs Sm/Yb diagram. Primitive mantle data from Hofmann (1988), continental crust, middle ocean rift basalt (MORB), ocean island basalts (OIB) and arc volcanic data from Schmidberger & Hegner (1999). Adakite field according to Richards & Kerrich (2007), Adakite-like rocks of the eastern Sakarya Zone from Topuz *et al.* (2005, 2011) and Dokuz *et al.* (2013). Non-adakitic rocks of the eastern Sakarya Zone from Aydınçakır (2014), Kaygusuz & Öztürk (2015) and Dokuz *et al.* (2019). Andean orogenic arc data from Petford & Atherton (1996) and Haschke *et al.* (2002).

The mafic microgranular enclaves are the most important indicator of the mixture of newly advected basic magma derived from the mantle with the fractionated and partly crystallized previous magma (Barbarin & Didier, 1992).

In the primitive mantle- and chondrite-normalized diagrams, pronounced negative anomalies are shown in Nb, P and Ti, and positive anomalies in Rb, Th, K and Pb, and enrichments in LILEs and light REEs relative to the HFSE and heavy REEs. These features are generally typical for the rocks with mantle wedge and crustal origin. I-type and high-K nature of the rocks can be formed by the partial melting of calc-alkaline basic and intermediate rocks in the crust (Roberts & Clemens, 1993). Magmas derived from these sources may produce granitic rocks via FC and/or crustal contamination. Granitic composition may also be produced by low degree of partial melting of the basic lower crust (Roberts & Clemens, 1993). The studied rocks display a wide range of Y/Nb ratio (1.73 to 5.48). This implies both the mantle and crustal origins for the rocks because Y/Nb ratio is lower than 1.2 for mantle rocks and higher than 1.2 for crustal rocks (Eby, 1992). Nb/Ta ratio is 17.5 for the rocks originated from the mantle and is in between 11 and 12 for the magmas derived from the crustal igneous protoliths (Green, 1995). The Nb/Ta ratios of the studied samples are between 9.40 and 16.00, consistent with both the mantle and crustal rocks as a source. The absence of a clear differentiation in the medium and heavy REEs and low Sr/Y ratios (6.9 to 22.7) indicate that garnet was not a phase in the magma source (Fig. 8b).

The studied rocks are located in the lithospheric mantle field in the Nb/La versus La/Yb diagram (Fig. 13c) and close to the point of

https://doi.org/10.1017/S001675682300033X Published online by Cambridge University Press

average lower crustal rocks. However, on the Ce/Pb versus Ce diagram (Fig. 13d), the samples display a large variation from MORB+OIB field to continental crust (arc volcanics) due to the decreasing Ce/Pb ratios.

The Eocene post-collisional magmatism in the eastern Sakarya Zone has been separated into two: an early Eocene adakite-like (Topuz *et al.* 2005, 2011; Dokuz *et al.* 2013) and middle Eocene non-adakite-like (Aydınçakır, 2014; Dokuz *et al.* 2019). In the SiO_2 versus Sr/Y diagram, our samples are located in the field of normal arc rocks but closer to the field of the early-middle Eocene adakitic rocks (Fig. 13e). The La/Sm and Sm/Yb ratios of the rocks vary from 3.75 to 8.97 and 1.38 to 1.92, respectively, while the adakitic rocks are in between 7.3 to 10.6 and 2.3 to 7.6 (Fig. 13f). These La/Sm and Sm/Yb ratios are different from those of the Andean-type arc rocks.

The Sm-Nd model ages of the studied rocks are Neoproterozoic (0.83 Ga) and Mesoproterozoic (0.81–1.02 Ga), and their Pb isotope compositions are characteristically similar to those of the sub-continental crust.

The samples having high and positive $\epsilon Hf_{(t)}$ values (0.14 to 10.26; mean 4.53) match with those derived from an enriched mantle source and with minor crustal contamination. That $\epsilon Hf_{(t)}$ values cluster between 4 and 7, while 1.07 and 12 are obtained only in one analysis; these values are consistent with zircon formation from relatively juvenile magmas. Consistent with Th/U values, much of which generally have Th/U < 0.1, indicative of a probable magmatic origin (Fig. 5c). All these features indicate the derivation of the Dağdibi Pluton from a juvenile source.

5.f. Tectonic setting

The rocks of the Dağdibi Pluton have I-type and high K calc-alkaline character. They are enriched in LREE (Rb, Ba and K) and poor in HREE (Nb and Ti). All these features are typical for the rocks formed in arc settings (Floyd & Winchester, 1975; Rogers & Hawkesworth, 1989; Sajona *et al.* 1996). However, it is worth to remember here that the rocks formed during the post-collisional stages could also show subduction-related features (Roberts & Clemens, 1993). Hence, the results obtained from the tectonic discrimination diagrams do not always provide a clear distinction for the middle Eocene rocks of the eastern Sakarya Zone and need to be evaluated together with sedimentological, stratigraphical and structural data.

5.g. Geodynamic implications

There is a substantial consensus on that the northern branch of the Neotethys Ocean was closed by a northward subduction beneath the Sakarya Zone in Turkey (Şengör & Yılmaz, 1981) and can be followed by its oceanic remnants along the İzmir-Ankara-Erzincan Suture (Okay & Tüysüz, 1999). Although docking of the Anatolides with the Sakarya Zone happened at a time around the Late Cretaceous (latest Campanian), the hard collision did not occur until the Palaeocene, based on the regional stratigraphy. This is the conclusion of almost all the geologists who studied the region (e.g., Şengör & Yılmaz, 1981; Okay & Tüysüz, 1999; Okay *et al.* 2001; Topuz *et al.* 2005; Sosson *et al.* 2010; Karslı *et al.* 2011; Dokuz *et al.* 2019; Kandemir *et al.* 2019). Final igneous products of this oceanic closure display a relatively K-rich nature compared to those formed in its earlier stages (Karslı *et al.* 2018; Aydın *et al.* 2020; Oğuz-Saka *et al.* 2023). The Sakarya Zone and the Anatolides have stayed under the effects of a compressional regime throughout the Palaeocene-early Eocene. (Kandemir *et al.* 2019). Adakite-like rocks are the first igneous products of this syn- to post-collisional period (Dokuz *et al.* 2013, 2019; Gücer, 2021). They intruded into the crust in the early Eocene (55–50 Ma) following a magmatic lull up to 10 to 12 Ma after the final subduction-related products at around 72 Ma (Topuz *et al.* 2005; Eyüboğlu *et al.* 2011; Karslı *et al.* 2011). This period was followed by a non-adakitic igneous activity in the middle Eocene without any gap. The igneous products show a range in age from 50 to 43 Ma and carry more or less geochemical features identical to those formed in arc settings (Dokuz *et al.* 2019; Sipahi *et al.* 2022; this study). The subduction imprints are diminished or completely erased in the rocks formed in the age span of 43 to 36 Ma (Eyüboğlu *et al.* 2017; Dokuz *et al.* 2019). The rocks of this time span commonly have hybrid geochemical characteristics taken from both the subduction and upwelling asthenosphere.

There are various geodynamic models proposed for the explanation of the Early Cenozoic post-collisional magmatism in the eastern Sakarya Zone. These are melting of lower crust due to the crustal thickening (Topuz *et al.* 2005), lithospheric delamination (e.g. Arslan *et al.* 2013; Temizel *et al.* 2016) and slab break-off (e.g. Keskin *et al.* 2008; Dilek *et al.* 2010; Altunkaynak *et al.* 2012; Dokuz *et al.* 2019; Gücer, 2021). The authors consider that the slab-breakoff model best explains the Early Cenozoic post-collisional magmatism in the Sakarya Zone as outlined in Dokuz *et al.* (2019).

6. Conclusions

U–Pb SHRIMP zircon ages (45.01 ± 0.59 Ma and 44.75 ± 0.92 Ma) indicate that the Dağdibi Pluton in the eastern Sakarya Zone, Turkey, is one of the small members of the large plutonic activity in the middle Eocene. The rocks of the pluton vary in composition from diorite through granodiorite to granite and display high-K calc-alkali, metaluminous and I-type affinities. Plagioclase shows a compositional range from labradorite (An_{62}) to oligoclase (An_{10}). Fractionation of plagioclase, hornblende and Fe-Ti oxide was effective during the formation of the pluton. Disequilibrium textures, curvilinear variations of element ratios and mafic magmatic enclaves are regarded as the indicators of magma mixing. Mineral compositions and P–T estimations show that the parental magma of the pluton was emplaced at ~3 to 6 km crustal depths and crystallized at temperatures of 625 and 792 °C. Slab breakoff, which occurred approximately 10 to 12 Ma after the collision of Anatolide-Tauride Block with the Sakarya Zone in the Late Cretaceous (late Campanian), is regarded as the geodynamic process responsible for the formation of the middle Eocene magmatism in the eastern Sakarya Zone.

Supplementary material. To view supplementary material for this article, please visit https://doi.org/10.1017/S001675682300033X

Acknowledgements. This study was supported by Gümüşhane University, Scientific Research Projects Coordination Department (Project numbers: 19.F5114.01.03 and 19.F5114.07.04) and a TÜBİTAK Project (number: 114Y099). Authors thank Tanju Aydurmuş for help during the field studies. Also, we would like to thank the editor, Dr. Tim Johnson, and the reviewers, Dr. Gültekin Topuz and Dr. Aral Okay, for their important contributions.

References

Abdel-Fattah MA (1994) Nature of biotites from alkaline, calc-alkaline, and peraluminous magmas. *Journal of Petrology* **35**, 525–41.

Altunkaynak Ş, Sunal G, Aldanmaz E, Genç CŞ, Dilek Y, Furnes H, Foland KA, Yang J and Yıldız M (2012) Eocene Granitic Magmatism in NW

Anatolia (Turkey) revisited: new implications from comparative zircon SHRIMP U–Pb and ^{40}Ar–^{39}Ar geochronology and isotope geochemistry on magma genesis and emplacement. *Lithos* **155**, 289–309.

Andersen DJ and Lindsley DH (1985) New (and final!) models for the Ti-magnetite/ilmenite geothermometer and oxygen barometer. *EOS Transactions American Geophysical Union* **66**, 416.

Anderson JL and Smith DR (1995) The effects of temperature and fO_2 on the Al-in-hornblende barometer. *American Mineralogist* **80**, 549–59.

Arslan M and Aslan Z (2006) Mineralogy, petrography and whole-rock geochemistry of the Cenozoic granitic intrusion in the Eastern Pontides (Turkey). *Journal of Asian Earth Sciences* **27**, 177–93.

Arslan M, Temizel İ, Abdioğlu E, Kolaylı H, Yücel C, Boztuğ D and Şen C (2013) ^{40}Ar–^{39}Ar dating, whole-rock and Sr–Nd–Pb isotope geochemistry of post-collisional Eocene volcanic rocks in the southern part of the Eastern Pontides (NE Turkey): implications for magma evolution in extension-induced origin. *Contributions to Mineralogy and Petrology*, **166**, 113–42.

Aydın F, Oğuz Saka S, Şen C, Dokuz A, Aiglsperger T, Uysal İ, Kandemir R, Karslı O, Sarı B and Başer R (2020) Temporal, geochemical and geodynamic evolution of the late Cretaceous subduction zone volcanism in the eastern Sakarya Zone, NE Turkey: implications for mantle-crust interaction in an arc setting. *Journal of Asian Earth Sciences* **192**, 104217.

Aydınçakır E (2014) The petrogenesis of Early Eocene non-adakitic volcanism in NE Turkey: constraints on the geodynamic implications. *Lithos* **208**, 361–77.

Bacon CR and Hirschmann MM (1988) Mg/Mn partitioning as a test for equilibrium between coexisting Fe-Ti oxides. *American Mineralogist* **73**, 57–61.

Barbarin B (1999) A review of the relationships between granitoid types, their origins and their geodynamic environments. *Lithos* **46**, 605–26.

Barbarin B and Didier J (1992) Genesis and evolution of mafic microgranular enclaves through various types of interaction between coexisting felsic and mafic magmas. *Transactions of the Royal Society of Edinburgh Earth Sciences* **83**, 145–53.

Blundy JD and Holland TJB (1990) Calcic amphibole equilibria and a new amphibole-plagioclase geothermometer. *Contributions to Mineralogy and Petrology* **104**, 208–24.

Boynton WV (1984) Cosmochemistry of the rare earth elements; meteorite studies. In Rare Earth Element Geochemistry (ed P Henderson), pp. 63–114. Amsterdam: Elsevier.

Boztuğ D, Jonckheere R, Wagner GA and Yeğingil Z (2004) Slow Senonian and fast Palaeocene-early Eocene uplift of the granitoids in the central Eastern Pontides, Turkey: apatite fission-track results. *Tectonophysics* **382**, 213–28.

Boztuğ D, Jonckheere RC, Wagner GA, Erçin Aİ and Yeğingil Z (2007) Titanite and zircon fission-track dating resolves successive igneous episodes in the formation of the composite Kaçkar batholith in the Turkish Eastern Pontides. *International Journal of Earth Sciences* **96**, 875–86.

Chappell BW and White AJR (1992) I- and S-type granites in the Lachlan fold belt. *Earth and Environmental Science Transactions of the Royal Society of Edinburgh* **83**, 1–26.

Chu NC, Taylor RN, Chavagnac V, Nesbitt RW, Boella M and Milton JA (2002) Hf isotope ratio analysis using multi-collector inductively coupled plasma mass spectrometry: an evaluation of isobaric interference corrections. *Journal of Analytical Atomic Spectrometry* **17**, 1567–74.

Delaloye M, Çoğulu E and Chessex R (1972) Etude ge'ochronometrique des massifs cristallins de Rize et de Gümüşhane, Pontides Orientales Turquie. *Archives des Sciences Physiques et Naturelles* **25** (Suppl.7(2–3)), 43–52.

Dilek Y, Imamverdiyev N and Altunkaynak Ş (2010) Geochemistry and tectonics of Cenozoic volcanism in the Lesser Caucasus (Azerbaijan) and the peri-Arabian region: collision-induced mantle dynamics and its magmatic fingerprint. *International Geology Review* **52**, 536–78.

Dokuz A (2011) A slab detachment and delamination model for the generation of Carboniferous high-potassium I-type magmatism in the Eastern Pontides, NE Turkey: the Köse composite pluton. *Gondwana Research* **19**, 926–44.

Dokuz A, Alçiçek MC, Tunçdemir V, Kandemir R and Aydınçakır E (2023) Post-Variscan autochthonous cover in the eastern Sakarya Zone, Turkey: evolution of the late Carboniferous back-arc ocean to the Triassic Karakaya Ocean. *Journal of Asian Earth Sciences* **249**, 105621.

Dokuz A, Aydin F and Karslı O (2019) Postcollisional transition from subduction- to intraplate-type magmatism in the eastern Sakarya zone, Turkey: indicators of northern Neotethyan slab breakoff. *GSA Bulletin* **131**, 1623–42.

Dokuz A, Aydınçakır E, Kandemir R, Karslı O, Siebel W, Derman AS and Turan M (2017b) Late Jurassic Magmatism and Stratigraphy in the Eastern Sakarya Zone, Turkey: evidence for the Slab Breakoff of Paleotethyan Oceanic lithosphere. *The Journal of Geology* **125**, 1–31.

Dokuz A, Gücer MA, Karslı O and Yi K (2022) From Cadomian back-arc basin to Rheic Ocean closure: the geochronological records of the Kurtoğlu Massif, eastern Sakarya zone, Turkey. *International Journal of Earth Sciences* **111**, 1333–55.

Dokuz A, Külekçi E, Aydınçakır E, Kandemir R, Alçiçek MC, Pecha ME and Sünnetçi K (2017a) Cordierite-bearing strongly peraluminous Cebre Rhyolite from the eastern Sakarya Zone, NE Turkey: constraints on the Variscan Orogeny. *Lithos* **278–281**, 285–302.

Dokuz A and Sünnetçi K (2019) Jurassic acidic magmatism in a back-arc setting, eastern Sakarya Zone, Turkey: geochemical constraints and an evolutionary model. *Lithos* **332–333**, 312–27.

Dokuz A and Tanyolu E (2006) Geochemical constraints on the provenance, mineral sorting and subaerial weathering of Lower Jurassic and Upper Cretaceous clastic rocks from the eastern Pontides, Yusufeli (Artvin), NE Turkey. *Turkish Journal of Earth Sciences* **15**, 181–209.

Dokuz A, Tanyolu E and Genç S (2006) A mantle- and a lower crust-derived bimodal suite in the Yusufeli (Artvin) area, NE Turkey: trace element and REE evidence for subduction-related rift origin of Early Jurassic Demirkent intrusive complex. *International Journal of Earth Sciences* **95**, 370–94.

Dokuz A, Uysal İ, Siebel W, Turan M, Duncan R and Akcay M (2013) Post-collisional adakitic volcanism in the eastern part of the Sakarya Zone, Turkey: evidence for slab and crustal melting. *Contributions to Mineralogy and Petrology* **166**, 1443–68.

Droop GTR (1987) A general equation for estimating Fe^{3+} concentrations in ferromagnesian silicates and oxides from microprobe analyses, using stoichiometric criteria. *Mineralogical Magazine* **51**, 431–5.

Eby GN (1992) Chemical subdivision of the A-type granitoids: petrogenetic and tectonic implications. *Geology* **20**, 641–4.

Eyüboğlu Y, Dudas FO, Santosh M, Zhuc DC, Yi K, Chatterjee N, Jeong YJ, Akaryalı E and Liuc Z (2016) Cenozoic forearc gabbros from the northern zone of the Eastern Pontides Orogenic Belt, NE Turkey: implications for slab window magmatism and convergent margin tectonics. *Gondwana Research* **33**, 160–89.

Eyüboğlu Y, Dudas FO, Thorkelson D, Zhu DC, Liu Z, Chatterjee N, Yi K and Santosh M (2017) Eocene granitoids of northern Turkey: Polybaric magmatism in an evolving arc–slab window system. *Gondwana Research* **50**, 311–45.

Eyüboğlu Y, Santosh M and Chung SL (2011) Petrochemistry and U-Pb Zircon ages of Adakitic Intrusions from the Pulur Massif (Eastern Pontides, NE Turkey): implications for Slab Rollback and ridge subduction associated with Cenozoic Convergent Tectonics in the Eastern Mediterranean. *The Journal of Geology* **119**, 394–417.

Floyd PA and Winchester JA (1975) Magma type and tectonic setting discrimination using immobile elements. *Earth and Planetary Science Letters* **27**, 211–8.

Frost BR, Barnes CG, Collins WJ, Arculus RJ, Ellis DJ and Frost CD (2001) A geochemical classification for granitic rocks. *Journal of Petrology* **42**, 2033–48.

Göçmengil G, Karacık Z, Genç ŞC and Billor MZ (2018) ^{40}Ar-^{39}Ar geochronology and petrogenesis of postcollisional trachytic volcanism along the İzmir-Ankara-Erzincan Suture zone (NE, Turkey). *Turkish Journal of Earth Sciences* **27**, 1–31.

Graham CM (1974) Metabasite amphibolites of the Scottish Dalradian. *Contributions to Mineralogy and Petrology* **47**, 165–85.

Green TH (1995) Significance of Nb/Ta as an indicator of geochemical processes in the crust-mantle system. *Chemical Geology* **120**, 347–59.

Griffin WL, Pearson NJ, Belousova E, Jackson SE, van Achtersergh E, O'Reilly SY and Shee SR (2000) The Hf isotope composition of cratonic mantle: LAM-MC-ICPMS analysis of zircon megacrysts in Kimberlites. *Geochimica et Cosmochimica Acta* **64**, 133–47.

https://doi.org/10.1017/S001675682300033X Published online by Cambridge University Press

Grove TL and Donnelly-Nolan JM (1986) The evolution of young silicic lavas at medicine Lake Volcano, California: implications for the origin of compositional gaps in calc-alkaline series lavas. *Contributions to Mineralogy and Petrology* **92**, 281–302.

Gücer MA (2021) Origin, petrogenesis and geodynamic implications of the early Eocene Altınpınar adakitic andesites in the eastern Sakarya Zone, northeastern Turkey. *Geochemistry* **81**, 125766.

Gücer MA, Aydınçakır E, Yücel C and Akaryalı E (2017) Tersiyer yaşlı Altınpınar hornblendli andezitlerinin (Torul-Gümüşhane) petrografisi, mineral kimyası ve P-T kristalleşme koşulları. *Gümüşhane Üniversitesi, Fen Bilimleri Dergisi* **7**, 236–67 (in Turkish with English abstract).

Hammarstrom JM and Zen E (1986) Aluminum in amphibole: an empirical igneous geobarometer. *American Mineralogist* **71**, 1297–313.

Hanchar JM and Watson EB (2003) Zircon saturation thermometry. *Reviews in Mineralogy and Geochemistry* **53**, 89–112.

Hart SR (1984) A large-scale isotope anomaly in the Southern Hemisphere mantle. *Nature* **309**, 753–7.

Haschke M, Siebel W, Günther A and Scheuber E (2002) Repeated crustal thickening and recycling during the Andean orogeny in the north Chile (21°–26°S). *Journal of Geophysical Research: Solid Earth* **107**, 1–18.

Helmy HM, Ahmed AF, El Mahallawi MM and Ali SM (2004) Pressure, temperature and oxygen fugacity conditions of calc-alkaline granitoids, Eastern Desert of Egypt, and tectonic implications. *Journal of African Earth Sciences* **38**, 255–68.

Hildreth W and Moorbath S (1988) Crustal contributions to arc magmatism in the Andes of Central Chile. *Contributions to Mineralogy and Petrology* **98**, 455–89.

Hofmann AW (1988) Chemical differentiation of the Earth: the relationship between mantle, continental crust, and oceanic crust. *Earth and Planetary Science Letters* **90**, 297–314.

Hollister LS, Grisson GC, Peters EK, Stowel HH and Sisson VB (1987). Confirmation of the empirical calibration of Al in hornblende with pressure of solidification of calc-alkaline plutons. *American Mineralogist* **72**, 231–9.

Iizuka T and Hirata T (2005) Improvements of precision and accuracy in in-situ Hf isotope microanalysis of zircon using the laser ablation-MC-ICPMS technique. *Chemical Geology* **220**, 121–37.

JICA (1986) The republic of Turkey report on the cooperative mineral exploration of Gümüşhane area, consolidated report. In *Japanese International Cooperation Agency*, p. 146. Ankara, Turkey: (unpublished), MTA Report.

Johnson MC and Rutherford MJ (1989) Experimental calibration of the aluminum-in-hornblende geobarometer with application to Long Valley caldera (California) volcanic rocks. *Geology* **17**, 837–41.

Kandemir Ö, Akbayram K, Çobankaya M, Kanar F, Pehlivan Ş, Tok T, Hakyemez A, Ekmekçi E, Danacı F and Temiz U (2019) From arc evolution to arc-continent collision: late Cretaceous–middle Eocene geology of the Eastern Pontides, northeastern Turkey. *GSA Bulletin* **131**, 1889–906.

Karslı O, Aydin F, Uysal İ, Dokuz A, Kumral M, Kandemir R, Budakoğlu M and Ketenci M (2018) Latest Cretaceous "A2-type" granites in the Sakarya Zone, NE Turkey: partial melting of mafic lower crust in response to roll-back of Neo-Tethyan oceanic lithosphere. *Lithos* **302–303**, 312–28.

Karslı O, Chen B, Aydin F and Şen C (2007) Geochemical and Sr–Nd–Pb isotopic compositions of the Eocene Dölek and Sariçiçek Plutons, Eastern Turkey: implications for magma interaction in the genesis of high-K calc-alkaline granitoids in a post-collision extensional setting. *Lithos* **98**, 67–96.

Karslı O, Dokuz A and Kandemir R (2017) Zircon Lu-Hf isotope systematics and U–Pb geochronology, whole-rock Sr-Nd isotopes and geochemistry of the early Jurassic Gokcedere pluton, Sakarya Zone-NE Turkey: a magmatic response to roll-back of the Paleo-Tethyan oceanic lithosphere. *Contributions to Mineralogy and Petrology* **172**, 31.

Karslı O, Dokuz A, Uysal İ, Aydin F, Kandemir R and Wijbrans J (2010) Generation of the Early Cenozoic adakitic volcanism by partial melting of mafic lower crust, Eastern Turkey: implications for crustal thickening to delamination. *Lithos* **114**, 109–20.

Karslı O, Dokuz A, Uysal İ, Ketenci M, Chen B and Kandemir R (2012) Deciphering the shoshonitic monzonites with I-type characteristic, the Sisdağı pluton, NE Turkey: magmatic response to continental lithospheric thinning. *Journal of Asian Earth Sciences* **51**, 45–62.

Karslı O, Ketenci M, Uysal İ, Dokuz A, Aydin F, Chen B, Kandemir R and Wijbrans J (2011) Adakite-like granitoid porphyries in the Eastern Pontides, NE Turkey: potential parental melts and geodynamic implications. *Lithos* **127**, 354–72.

Kaygusuz A, Arslan M, Siebel W, Sipahi F, İlbeyli N and Temizel İ (2014) LA-ICP MS zircon dating, whole-rock and Sr–Nd–Pb–O isotope geochemistry of the Camiboğazı pluton, Eastern Pontides, NE Turkey: implications for lithospheric mantle and lower crustal sources in arc-related I-type magmatism. *Lithos* **192–195**, 271–90.

Kaygusuz A, Arslan M, Wolfgang S, Sipahi F and İlbeyli N (2012) Geochronological evidence and tectonic significance of Carboniferous magmatism in the southwest Trabzon area, eastern Pontides, Turkey. *International Geology Review* **54**, 1776–1800.

Kaygusuz A and Öztürk M (2015) Geochronology, geochemistry, and petrogenesis of the Eastern Pontides, NE Turkey: evidence for lithospheric mantle and lower crustal sources in the high-K calc-alkaline magmatism. *Journal of Asian Earth Sciences* **108**, 97–116.

Kaygusuz A, Yücel C, Arslan M, Sipahi F, Temizel İ, Çakmak G and Güloğlu ZS (2018) Petrography, mineral chemistry and crystallization conditions of Cenozoic plutonic rocks located to the north of Bayburt (Eastern Pontides, Turkey). *Bulletin of the Mineral Research and Exploration* **157**, 75–102.

Kaygusuz A, Yücel C, Arslan M, Temizel İ, Yi K, Jeong Y-J, Siebel W and Sipahi F (2020) Eocene I-type magmatism in the Eastern Pontides, NE Turkey: insights into magma genesis and magma-tectonic evolution from whole-rock geochemistry, geochronology and isotope systematics. *International Geology Review* **62**, 1406–32.

Kemp AIS (2004) Petrology of high-Mg igneous rocks of the Glenelg River complex, southeastern Australia, and the nature of their interaction with crustal melts. *Lithos* **78**, 119–56.

Kempton PD, Downes H and Embey-Istzin A (1997) Mafic granulite xenoliths in Neogene alkali basalts from the western Pannonian basin: insights into the lower crust of a collapsed orogen. *Journal of Petrology* **38**, 941–70.

Keskin M, Genç ŞC and Tüysüz O (2008) Petrology and geochemistry of post-collisional Middle Eocene volcanic units in North-Central Turkey: evidence for magma generation by slab breakoff following the closure of the Northern Neotethys Ocean. *Lithos* **104**, 267–305.

Le Maitre RW (1989) *A Classification of Igneous Rocks and Glossary of Terms*. Recommendations of the IUGS Commission on the systematics of igneous rocks. Oxford: Blackwell Scientific Publications, 193 pp.

Leake BE (1964) The chemical distinction between ortho- and para-amphibolites. *Journal of Petrology* **5**, 238–54.

Leake BE, Wooley AR, Arps CES, Birch WD, Gilbert MC, Grice JD, Hawthorne FC, Kato A, Kisch HJ, Krivovichev VG, Linthout K, Laird J, Mandarino JA, Maresch WV, Nickhel EH, Rock NMS, Schumacher JC, Smith DC, Stephenson NCN, Ungaretti L, Whittaker EJW and Youzhi G (1997) Nomenclature of Amphiboles. *American Mineralogist* **82**, 1019–37.

Lepage LD (2003) ILMAT: an Excel worksheet for ilmenite–magnetite geothermometry and geobarometry. *Computers & Geosciences* **29**, 673–8.

Ludwig KR (2012) *User's Manual for Isoplot 4.15 A Geochronological Toolkit for Microsoft Excel*. Berkeley, CA: Berkeley Geochronology Center Special Publication no. 5, 75p.

Luhr JF (1992) Slab-derived fluids and partial melting in subduction zones: insights from two contrasting Mexican volcanoes (Colima and Ceboruco). *Journal of Volcanology and Geothermal Research* **54**, 1–18.

Luhr JF, Carmichael ISE and Varekamp JC (1984) The 1982 eruptions of El Chicón Volcano, Chiapas, Mexico: mineralogy and petrology of the anhydrite-bearing pumices. *Journal of Volcanology and Geothermal Research* **23**, 69–108.

Mason PRD, Downes H, Thirlwall MF, Seghedi I, Szakacs A, Mattey DP and Lowery D (1996) Crustal contamination as a major petrogenetic process in the East Carpathian Neogene and Quaternary continental margin arc, Romania. *Journal of Petrology* **37**, 927–60.

McCulloch MT and Gamble JA (1991) Geochemical and geodynamical constraints on subduction zone magmatism. *Earth and Planetary Science Letters* **102**, 358–74.

Merzbacher C and Eggler DH (1984) A magmatic geohygrometer: application to Mount St. Helens and other dacitic magmas. *Geology* **12**, 587–90.

Middlemost EAK (1994) Naming materials in the magma/igneous rock system. *Earth-Science Reviews* **37**, 215–24.

Miller CF, McDowell SM and Mapes RW (2003) Hot and cold granites? Implications of zircon saturation temperatures and preservation of inheritance. *Geology* **31**, 529–32.

Moore WJ, Mckee EH and Akıncı Ö (1980) Chemistry and chronology of plutonic rocks in the Pontid Mountains, Northern Turkey. In *Symposium of European Copper Deposits*, (eds S Jankovic and RH Sillitoe), pp. 209–16. Belgrade, Serbia.

Moritz R, Popkhadze N, Hässig M, Golay T, Lavoie J, Gugushvili V, Ulianov A, Ovtcharova M, Grosjean M, Chiaradia M and Dumitrica P (2020) At the crossroads of the Lesser Caucasus and the Eastern Pontides: late Cretaceous to early Eocene magmatic and geodynamic evolution of the Bolnisi district, Georgia. *Lithos* **378–379**, 105872.

Mutch EJF, Blundy JD, Tattitch BC, Cooper FJ and Brooker RA (2016) An experimental study of amphibole stability in low-pressure granitic magmas and a revised Al-in-hornblende geobarometer. *Contributions to Mineralogy and Petrology* **171**, 85.

Oğuz-Saka S, Aydin F, Karsli O, Dokuz A, Aiglsperger T, Miggins DP, Şen C, Kandemir R, Sarı B and Koppers AAP (2023). Two-stage bimodal volcanism in a Late Cretaceous arc/back-arc setting, NE Turkey: constraints from volcano-stratigraphy, zircon U-Pb and $^{40}Ar/^{39}Ar$ geochronology and whole-rock elemental and Sr-Nd-Pb isotope geochemistry. *Lithos* **440–441**, 107018.

Okay Aİ and Leven EJ (1996) Stratigraphy and paleontology of the upper Paleozoic sequences in the Pulur (Bayburt) region, Eastern Pontides. *Turkish Journal of Earth Sciences* **5**, 145–55.

Okay Aİ, Tansel İ and Tüysüz O (2001) Obduction, subduction and collision as reflected in the Upper Cretaceous–Lower Eocene sedimentary record of western Turkey. *Geological Magazine* **138**, 117–42.

Okay Aİ, Topuz G, Kylander-Clark ARC, Sherlock S and Zattin M (2022) Late Paleocene – Middle Eocene magmatic flare-up in western Anatolia. *Lithos* **428–429**, 106816.

Okay Aİ and Tüysüz O (1999) Tethyan sutures of northern Turkey. In *The Mediterranean Basins: Tertiary Extension within the Alpine Orogen Tethyan Sutures of Northern Turkey* (eds B Durand, L Jolivet, F Hovarth and M Séranne), pp. 475–515. Geological Society of London, Special Publications no. 156, UK.

Paces JB and Miller JD (1993) Precise U-Pb ages of Duluth Complex and related mafic intrusions, northeastern Minnesota: Geochronological insights to physical, petrogenetic, paleomagnetic, and tectonomagmatic processes associated with the 1.1 Ga Midcontinent Rift System. *Journal of Geophysical Research: Solid Earth* **98**, 13997–14013.

Patchett PJ, Kuovo O, Hedge CE and Tatsumoto M (1981) Evolution of continental crust and mantle heterogeneity: evidence from Hf isotopes. *Contributions to Mineralogy and Petrology* **78**, 279–97.

Patiño Douce AE and Johnston AD (1991) Phase equilibria and melt productivity in the pelitic system: implications for the origin of peraluminous granitoids and aluminous granulites. *Contributions to Mineralogy and Petrology* **107**, 202–18.

Paton C, Hellstrom J, Paul B, Woodhead J and Hergt J (2011) Iolite: freeware for the visualization and processing of mass spectrometric data. *Journal of Analytical Atomic Spectrometry* **26**, 2508–18.

Perugini D and Poli G (2004) Determination of the degree of compositional disorder in magmatic enclaves using SEM, X-ray element, maps. *European Journal of Mineralogy* **16**, 431–42.

Petford N and Atherton A (1996) Na-rich partial melts from newly underplated basaltic crust: the Cordillera Blanca Batholith, Peru. *Journal of Petrology* **37**, 1491–521.

Ramos FC (1992) Isotope Geology of the Metamorphic Core of the Central Grouse Creek Mountains, Box elder Country, Utah. MSc thesis, University of California, Los Angeles.

Rapela CW and Pankhurst RJ (1996) Monzonite Suites: the innermost Cordilleran plutonism of Patagonia. *Transactions of the Royal Society of Edinburgh, Earth Sciences* **87**, 193–203.

Richards JP and Kerrich R (2007) Special Paper: Adakite-Like Rocks: their diverse origins and questionable role in metallogenesis. *Economic Geology* **102**, 537–76.

Ridolfi F, Renzulli A and Puerini M (2010) Stability and chemical equilibrium of amphibole in calc–Alkaline magmas: an overview, new thermobarometric formulations and application to subduction–related volcanoes: *Contributions to Mineralogy and Petrology* **160**, 45–66.

Roberts MP and Clemens JD (1993) Origin of high-potassium, calc-alkaline, I-type granitoids. *Geology* **21**, 825–8.

Rogers G and Hawkesworth CJ (1989) A geochemical traverse across the North Chilean Andes: evidence for crust generation from the mantle wedge. *Earth and Planetary Science Letters* **91**, 271–85.

Russel WA, Papanastassiou DA and Tombrello TA (1978) Ca isotope fractionation on the earth and other solar system materials. *Geochimica et Cosmochimica Acta* **42**, 1075–90.

Sajona FG, Maury RC, Bellon H, Cotten J and Defant M (1996) High field strength element enrichment of Pliocene-Pleistocene Island Arc Basalts, Zamboanga Peninsula, Western Mindanao (Philippines). *Journal of Petrology* **37**, 693–726.

Schmidberger S and Hegner E (1999) Geochemistry and isotope systematics of calc-alkaline volcanic rocks from the Saar-Nahe basin (SW Germany)-implications for Late-Variscan orogenic development. *Contributions to Mineralogy and Petrology* **135**, 373–85.

Schmidt MW (1992) Amphibole composition in tonalite as a function of pressure: an experimental calibration of the Al-in-hornblende barometer. *Contributions to Mineralogy and Petrology* **110**, 304–10.

Şengör AMC, Özeren S, Genç T and Zor E (2003) East Anatolian high plateau as a mantle-supported, north-south shortened domal structure. *Geophysical Research Letters* **30**, 8045.

Şengör AMC and Yılmaz Y (1981) Tethyan evolution of Turkey: a plate tectonic approach. *Techtonophysics* **75**, 181–241.

Sipahi F (2005) Zigana dağı (Torul-Gümüşhane) volkanitlerindeki hidrotermal ayrışmaların mineraloji ve jeokimyası. PhD thesis, Department of Geological Engineering, Karadeniz Technical University, Trabzon, Türkiye, 194 pp.

Sipahi F (2017) Kalınçam (Tonya-Trabzon, KD Türkiye) yöresi Geç Kretase yaşlı volkanitlerin jeokimyası ve petrojenezi. *Gümüşhane Üniversitesi Fen Bilimleri Dergisi* **7**, 102–27 (in Turkish with English abstract).

Sipahi F (2019) Nature of tourmaline formation in quartz porphyry in the E Sakarya zone (NE Turkey): geochemistry and isotopic approach. *Periodico di Mineralogia* **88**, 333–51.

Sipahi F, Akpınar İ, Saydam Eker Ç, Kaygusuz A, Vural A and Yılmaz M (2017) Formation of the Eğrikar (Gümüşhane) Fe–Cu skarn type mineralization in NE Turkey: U–Pb zircon age, lithogeochemistry, mineral chemistry, fluid inclusion, and O-H-C-S isotopic compositions. *Journal of Geochemical Exploration* **182**, 32–52.

Sipahi F, Gücer MA and Sadıklar MB (2020a) Nature of clays in Late Cretaceous dacitic rocks in the eastern Sakarya Zone (NE Turkey): a geochemical and isotopic approach. *Turkish Journal of Earth Sciences* **29**, 831–52.

Sipahi F, Gücer MA and Saydam Eker Ç (2020b) Geochemical composition of magnetite from different iron skarn mineralizations in NE Turkey: implication for source of ore forming fluids. *Arabian Journal of Geosciences* **13**, 70.

Sipahi F, Kaygusuz A, Saydam Eker Ç, Vural A and Akpınar İ (2018a) Late Cretaceous arc igneous activity: the Eğrikar Monzogranite example. *International Geology Review* **60**, 382–400.

Sipahi F and Sadıklar MB (2014) Geochemistry of dacitic volcanics in the eastern pontides (NE Turkey). *Geochemistry International* **4**, 329–49.

Sipahi F, Saydam Eker Ç, Akpınar İ, Gücer MA, Vural A, Kaygusuz A and Aydurmuş T (2022) Eocene magmatism and associated Fe-Cu mineralization in northeastern Turkey: a case study of the Karadağ skarn. *International Geology Review* **64**, 1530–55.

Sipahi F, Saydam Eker Ç, Kaygusuz A and Vural A (2018b) Granitoyidlere (Gümüşhane, KD Türkiye) Bağlı Gelişen Skarn Cevherleşmelerinin Jeolojisi, Jeokimyası ve Jeokronolojisinin Araştırılması. Tübitak Ar-Ge 1001 Projesi, No: 114Y099. (in Turkish with English abstract).

Sláma J, Košler J, Condon DJ, Crowley JL, Gerdes A, Hanchar JM, Horstwood SA, Morris GA, Nasdala L, Norberg N, Schaltegger U, Schoene B, Tubrett MN and Whitehouse MJ (2008) Plešvice zircon – a new natural reference material for U-Pb and Hf isotopic microanalysis. *Chemical Geology* **249**, 1–35.

https://doi.org/10.1017/S001675682300033X Published online by Cambridge University Press

Smith JV and Brown WL (1988) *Feldspar Minerals 1- Crystal Structures, Physical, Chemical and Micro-Textural Properties*. Berlin: Springer-Verlag, 828 pp.

Sosson M, Rolland Y, Müller C, Danelian T, Melkonyan R, Kekelia S, Adamia S, Babazadeh V, Kangarli T, Avagyan A, Galoyan G and Mosar J (2010) Subductions, obduction and collision in the Lesser Caucasus (Armenia, Azerbaijan, Georgia), new insights. In *Sedimentary Basin Tectonics from the Black Sea and Caucasus to the Arabian Platform* (eds M Sosson, N Kaymakcı, RA Stephenson, F Bergerat and V Starostenko), pp. 329–52: Geological Society, London, Special Publication 340, UK.

Speer JA (1987) Evolution of magmatic AFM mineral assemblages in granitoid rocks; the hornblende + melt = biotite reaction in the Liberty Hill Pluton, South Carolina. *American Mineralogist* **72**, 863–78.

Spencer KJ and Lindsley DH (1981) A solution model for coexisting iron-titanium oxides. *American Mineralogist* **66**, 1189–201.

Stacey JS and Kramers JD (1975) Approximation of terrestrial lead isotope evolution by a two-stage model. *Earth and Planetary Science Letters* **26**, 207–21.

Streckeisen AL (1976) Classification and nomenclature of igneous rocks. *Neues Jahrbuch für Mineralogie (Abhandlungen)* **107**, 144–240.

Sun S and McDonough WF (1989) Chemical and isotopic systematics of oceanic basalt: implications for mantle composition and processes. In *Magmatism in the Ocean Basins* (eds AD Saunders and MJ Norry), pp. 313–45: Geological Society of London, Special Publication no. 42, UK.

Taner MF (1977) Etuda géologique et pétrographique de la région de Güneyce-İkizdere, située au sud de Rize (Pontides orientales, Turquie), PhD thesis, Universite de Geneve, 180 pp.

Taylor SR and McLennan SM (1985) *The Continental Crust: Its Composition and Evolution*. Blackwell, Oxford, UK: Blackwell Scientific Publications, 312 pp.

Temizel İ, Arslan M, Ruffet G and Peucat JJ (2012) Petrochemistry, geochronology and Sr–Nd isotopic systematics of the Tertiary collisional and post-collisional volcanic rocks from the Ulubey (Ordu) area, eastern Pontide, NE Turkey: implications for extension-related origin and mantle source characteristics. *Lithos* **128**, 126–47.

Topuz G, Altherr R, Schwarz WH, Dokuz A and Meyer H-P (2007) Variscan amphibolite facies metamorphic rocks from the Kurtoğlu metamorphic complex (Gümüşhane area, Eastern Pontides, Turkey). *International Journal of Earth Sciences* **96**, 861–73.

Topuz G, Altherr R, Schwarz WH, Siebel W, Satir M and Dokuz A (2005) Postcollisional plutonism with adakite-like signatures: the Eocene Saraycık granodiorite (Eastern Pontides, Turkey), *Contributions to Mineralogy and Petrology* **150**, 441–55.

Topuz G, Okay Aİ, Altherr R, Schwarz WH, Siebel W, Zack T, Satır M and Şen C (2011) Post-collisional adakite-like magmatism in the Ağvanis Massif and implications for the evolution of the Eocene magmatism in the Eastern Pontides (NE Turkey), *Lithos* **125**, 131–50.

Vervoort JD, Patchett PJ, Söderlund U and Baker M (2004) Isotopic composition of Yb and the determination of Lu concentrations and Lu/Hf ratios by isotope dilution using MC-ICPMS. *Geochemistry Geophysics Geosystems* **5**, Q11002.

Watson EB and Harrison TM (1983) Zircon saturation revisited: temperature and composition effects in a variety of crustal magma types. *Earth and Planetary Science Letters* **64**, 295–304.

Williams IS and Hergt JM (2000) U–Pb dating of Tasmanian dolerites: a cautionary tale of SHRIMP analysis of high-U zircon. In *Beyond 2000: New Frontiers in Isotope Geoscience* (eds JD Woodhead, JM Hergt & WP Noble), pp. 185–188. Lorne, Australia: Abstracts and Proceedings.

Yavuz F (1999) A revised program for microprobe-derived amphibole analyses using the IMA rules. *Computers and Geosciences* **25**, 909–27.

Yılmaz S and Boztuğ D (1996) Space and time relations of three plutonic phases in the Eastern Pontides, Turkey. *International Geology Review* **38**, 935–56.

Zindler A and Hart SR (1986) Chemical geodynamics. *Annual Review of Earth and Planetary Sciences* **14**, 493–571.

https://doi.org/10.1017/S001675682300033X Published online by Cambridge University Press